

Copyright © 1981, by the author(s).
All rights reserved.

Permission to make digital or hard copies of all or part of this work for personal or classroom use is granted without fee provided that copies are not made or distributed for profit or commercial advantage and that copies bear this notice and the full citation on the first page. To copy otherwise, to republish, to post on servers or to redistribute to lists, requires prior specific permission.

CHAOTIC MOTION ALONG RESONANCE LAYERS IN
NEAR-INTEGRABLE HAMILTONIAN SYSTEMS WITH
THREE OR MORE FREEDOMS

by

M. A. Lieberman and J. L. Tennyson

Memorandum No. UCB/ERL M81/16

31 March 1981

ELECTRONICS RESEARCH LABORATORY
College of Engineering
University of California, Berkeley
94720

CHAOTIC MOTION ALONG RESONANCE LAYERS IN
NEAR-INTEGRABLE HAMILTONIAN SYSTEMS WITH
THREE OR MORE FREEDOMS

M. A. Lieberman and J. L. Tennyson

Department of Electrical Engineering and Computer Sciences
and the Electronics Research Laboratory
University of California, Berkeley, California 94720

ABSTRACT

Chaotic motion along resonance layers in phase space appears generically in near integrable Hamiltonian systems with three or more freedoms. Such motion is forbidden in systems with two freedoms, where only chaotic motion across resonance layers is generic. We review three mechanisms for chaotic motion along resonance layers: Arnold diffusion, modulational diffusion, and resonance streaming... The emphasis is on the geometry of the motion in the phase and action spaces, simple physical pictures of the mechanisms, and computational examples.

Research sponsored by the Office of Naval Research Contract N00014-79-C-0674, the National Science Foundation Grant ENG-78-26372 and the Department of Energy Contract DE-AS03-76F00034-PA# DE-ATOE-76ET53059.

1. INTRODUCTION

It is well-known that Hamiltonian systems with one freedom $H(p,q)$ are integrable. For two freedoms $H(p_1, p_2, q_1, q_2)$ integrability is exceptional. In general, resonances between the two freedoms lead to the formation of a dense set of resonance layers in the action space. Within each layer, a chaotic motion appears. Energy conservation prevents large excursions of the motion along the layer. Only motion across the layer is important. For an integrable system with a weak perturbation² the chaotic layers are isolated by KAM surfaces. Thus motion from one layer to another is forbidden. For strong perturbations, resonance layers can overlap, the intervening KAM surfaces being destroyed. A globally chaotic motion then develops, leading to large excursions in both actions over long times.

For three or more freedoms, strong perturbations also lead to overlap of resonance layers and globally chaotic motion. However, for weak perturbations, two new effects appear:

(1) Resonance layers are no longer isolated by KAM surfaces. Generically, the layers intersect, forming a connected web dense in the action space.

(2) Conservation of energy no longer prevents large chaotic motions of the actions along the layers over long times. As a result, large, long-time excursions of the actions along resonance layers are generic in systems with three or more freedoms. In contrast, such motions are forbidden in systems with two freedoms. Furthermore, the interconnection of the dense set of layers ensures that the chaotic motion, stepping from layer to layer can carry the system arbitrarily close to any region of the phase space consistent with energy conservation.

The interconnection of, and motion along layers lies at the heart of the chaotic phenomena which are reviewed here. We describe three different mechanisms for motion along resonance layers: Arnold diffusion, modulational diffusion and resonance streaming. These mechanisms have no analog in systems with one or two freedoms.

This review is in four parts. It is first desirable to consider the geometry of the $2N$ -dimensional phase space, the $2N-2$ dimensional surface of section, and various projections, such as the N -dimensional action space. The emphasis is on simple diagrams that illustrate the definition of the resonance layers and give meaning to the notion of motion "across" and "along" layers. Using these diagrams, the different layers which give rise to Arnold diffusion, modulational diffusion and resonance streaming will be described qualitatively.

After this, we review in some detail the mechanism of Arnold diffusion, which gives rise to chaotic motion along resonance layers. Arnold diffusion is universal, in that there is no critical perturbation strength. Furthermore, the chaotic motion is intrinsic, i.e., generated by the dynamics alone. The diffusion appears as chaotic motion along thin layers of stochasticity surrounding the separatrices associated with non-overlapping resonances. A model problem, that of a ball bouncing between a flat and a periodically rippled wall, is used to illustrate the diffusion. The case of many non-interacting resonances (Nekhoroshev regime) is described qualitatively using a second model problem.

While Arnold diffusion appears as chaotic motion along non-overlapping resonance layers, modulational diffusion results when the layers associated with adjacent resonances overlap. The resulting diffusion along the overlapping resonance layer is generally much greater than for Arnold diffusion. Again, the chaotic motion is intrinsic to the

dynamics; no external noise acts on the system. However, modulational diffusion is not universal. There is a critical perturbation strength below which adjacent resonances do not overlap. Modulational diffusion is generally found in systems which have a slow oscillation in one of the freedoms. We describe here the formation of modulational stochastic layers, and present recent numerical results illustrating the chaotic motion along such layers.

To conclude this review, we examine the effect of weak, external stochasticity in producing enhanced diffusion along a resonance layer. If the motion in the absence of external noise is oscillation within a resonance layer, then the classical transport due to external noise or dissipation can be strongly enhanced along the layer. This effect is called resonance streaming, and will be illustrated for a model Hamiltonian perturbed by dissipation and by noise.

2. ACTION AND PHASE SPACE

We consider first an integrable Hamiltonian system with N freedoms. In action-angle form

$$H_0 = H_0(\underline{I})$$

where \underline{I} is the N -tuple of actions. The motion in the $2N$ -dimensional phase space $(\underline{I}, \underline{\theta})$ is on an N -dimensional torus defined by the N -tuple of angles $\underline{\theta}$ conjugate to \underline{I} :

$$\underline{I}(t) = \underline{I}_0, \quad \underline{\theta}(t) = \underline{\omega}(\underline{I})t + \underline{\theta}_0 \quad (1)$$

where

$$\omega_j(\underline{I}) = \partial H_0 / \partial I_j \quad (2)$$

is the N -vector of unperturbed frequencies.

Action space--Fig. 1 shows the N-dimensional action space. For the unperturbed system the actions are conserved and each trajectory is a stationary point. One may define an N-1 dimensional energy surface by the condition

$$H_0(\underline{I}) = \alpha.$$

For example, for free particle motion in N-dimensions,

$$H_0 = \sum_{j=1}^N I_j^2,$$

the energy surfaces are spheres, as shown in the figure.

One may also define an N-1 dimensional resonance surface by the condition

$$\underline{m} \cdot \underline{\omega}(\underline{I}) = 0 \quad (3)$$

where \underline{m} is called the resonance vector and has integer components. Since there is a resonance surface for each resonance vector, these surfaces are dense in the action space. For the free particle, several resonance surfaces are shown as the flat planes in Fig. 1.

We consider now the effect of a small perturbation, periodic in θ :

$$H = H_0(\underline{I}) + \epsilon \sum_k V_k(\underline{I}) e^{i \underline{m}_k \cdot \underline{\theta}} \quad (4)$$

where k represents the sum over all resonance vectors \underline{m}_k . The motion in action space is

$$\dot{\underline{I}} = -\partial H / \partial \underline{\theta} = -i \epsilon \sum_k \underline{m}_k V_k e^{i \underline{m}_k \cdot \underline{\theta}} \quad (5)$$

we see that each component k drives an oscillation in \underline{I} in the direction \underline{m}_k . For most k 's the oscillation will be non-resonant

$$\underline{m}_k \cdot \underline{\theta}(t) \neq \text{const}$$

and the amplitude of the oscillation in I will be of order ϵ , as shown in Fig. 2a. However, for some value $k = R$ we may find a resonant motion

$$\underline{m}_R \cdot \underline{\theta}(t) = \psi_R = \text{const} \quad (6)$$

where ψ_R is the resonance phase. In the direction of \underline{m}_R , which we define to be the direction of the resonance action I_R , the amplitude of the oscillation is of order $\epsilon^{1/2}$. We then have the picture shown in Fig. 2b. The direction of \underline{m}_R in the action space describes the motion "across" the resonance layer.

As an example, Fig. 3 shows some resonance surfaces and energy surfaces for the two freedom Hamiltonian

$$H_0 = I_1^2 + (6I_2)^2.$$

The resonances surfaces, from (3), are lines in the action space given by

$$m_1 I_1 + 36m_2 I_2 = 0$$

Some of these (for $m_2 = 1$) are plotted in the figure. Note that since

$$\underline{m}_R \cdot \partial H_0 / \partial \underline{I} = 0$$

at resonance, a resonance vector \underline{m}_R lies in an energy surface, as shown in the figure. In general \underline{m}_R , the direction of the resonance action excursion, is not perpendicular to the resonance surface. It can be seen from Fig. 3 that even for arbitrary m_1 and m_2 , resonance surfaces do not intersect on a constant (non-zero) energy surface. This property is generic for systems with two freedoms.

For three or more freedoms, resonance surfaces generically intersect. We illustrate this in Fig. 4 for a free particle in

three dimensions

$$H_0 = (1/2)(I_1^2 + I_2^2 + I_3^2),$$

The resonance surfaces are planes which pass through the origin in action space. The two planes intersect at non-zero actions along a line, as shown in the figure. The resonance surfaces also intersect a spherical energy surface $H_0(\underline{I}) = \alpha$ in great circle meridians (for this example, the resonance vectors \underline{m}_R happen to lie perpendicular to the resonance planes). An energy-conserving motion from one resonance to another is possible. The motion may proceed along a meridian of one resonance to an intersection, turn sharply, and then more along a new meridian. This type of motion is generic to systems with three or more freedoms. The intersection of resonances in the constant energy surface generates a dense interconnected network, the so-called Arnold web. The web for this example is illustrated in Fig. 5, with all resonances shown for which $|m_j| \leq 2$.

Phase space--Now we consider the geometry of stochastic layers in the $2N$ -dimensional phase space. The layers, defined by (3) are surfaces having dimension $2N-1$. The KAM surfaces, being perturbed tori defined by the condition

$$\underline{I} = \text{const}$$

are N -dimensional. The interconnection of resonance layers into the Arnold web can then be understood geometrically. For $N \geq 3$, the $2N-1$ dimensional resonance surfaces cannot be isolated from each other by N dimensional KAM surfaces. The situation is analogous to that illustrated in Fig. 6, where KAM "lines" isolate regions of a plane, but do not separate a three dimensional volume into a distinct parts.

Now consider a projection of a resonance layer in phase space onto the two-dimensional surface defined by the resonance action I_R and resonance angle ψ_R . Fixing all other actions and angles, we obtain the usual picture, Fig. 7, showing the structure of a stochastic layer in cross section. The stochasticity forms around the separatrix associated with the resonance m_R . The layer thickness is of order $\epsilon^{1/2}$. Near resonance, the topology of KAM surfaces has changed. Close to resonance, the surfaces perturb to the ellipses shown in the two dimensional projection in Fig. 7.

If we look at a resonance layer in a three dimensional projection, adding an additional action variable I_S , we obtain the structure shown in Fig. 8. The resonance layer extends along the unprojected action I_S (although its properties, such as its thickness, may vary with I_S). The KAM surfaces near exact resonance appear as elliptical tubes within the layer. In this figure, I_S represents one of the $N-1$ action variables (excluding the resonance action I_R) which define motion along a layer.

The essential feature of the behavior within resonance layers for three or more freedoms is the existence of long-time chaotic motion along resonance layers; i.e., along I_S . It is easy to see that such motion cannot be driven by the dynamics in near-integrable systems with two freedoms. The change in the Hamiltonian is

$$\Delta H = \Delta H_0 + \epsilon \Delta H_1 = 0,$$

since energy is conserved. Thus

$$\Delta H_0 = \frac{\partial H_0}{\partial I_R} \Delta I_R + \frac{\partial H_0}{\partial I_S} \Delta I_S = \mathcal{O}(\epsilon) \quad (7)$$

But if the resonance action I_R is confined to the resonance layer

$$\Delta I_R = \mathcal{O}(\epsilon^{1/2}). \quad (8)$$

It follows that

$$\Delta I_S = \mathcal{O}(\epsilon^{1/2}),$$

and large excursions along resonance layers are forbidden.

For three freedoms, (7) is replaced by

$$\frac{\partial H_0}{\partial I_R} \Delta I_R + \frac{\partial H_0}{\partial I_S} \Delta I_S + \frac{\partial H_0}{\partial I_T} \Delta I_T = \mathcal{O}(\epsilon) \quad (9)$$

Even if (8) holds, large excursions in the two actions I_S and I_T along the resonance are possible, provided

$$\frac{\partial H_0}{\partial I_S} \Delta I_S + \frac{\partial H_0}{\partial I_T} \Delta I_T = \mathcal{O}(\epsilon^{1/2}).$$

In this review we describe three types of chaotic motion along resonance layers. For Arnold diffusion, intrinsic randomness drives a slow diffusion along the stochastic separatrix layer, as illustrated in Fig. 8. In resonance streaming, extrinsic diffusion or dissipation drives a migration through the elliptical KAM tubes within the stochastic separatrix layer. This situation is also shown in Fig. 8. In modulational diffusion, illustrated in Fig. 9, a slow modulation in one freedom can produce multiplets of sideband resonances. When these overlap, a thick stochastic layer is formed along which diffusive motion appears.

3. ARNOLD DIFFUSION

As we have seen, for a system with at least three freedoms, all stochastic separatrix layers are connected into a single complex network -- the Arnold web. The web consists of an intricate system of "freeways, streets, sidewalks, and cracks" that permeates the entire phase space. For an initial condition within the web, the subsequent stochastic motion will eventually intersect every finite region of the phase space, even the predominantly stable regions where the fraction of

stochastic initial conditions is small, and even in the limit as the perturbation strength $\epsilon \rightarrow 0$. This motion is the Arnold diffusion. The merging of stochastic trajectories into a single web was proved by Arnold³ for a specific nonlinear Hamiltonian. A general proof of the existence of a single web has not been given, but many computational examples are known.

From a practical point of view, there are two major questions concerning Arnold diffusion in a particular system:

- (1) what is the relative measure of stochastic trajectories in the phase space region of interest? and
- (2) for a given initial condition, how fast will the system diffuse along the thin threads of the Arnold web?

The extent of the web in phase space can be estimated by means of resonance overlap conditions⁴. Overlap of resonances near the separatrix gives rise to a resonance layer thickness, with stochastic motion occurring across the layer as in systems with two freedoms.

Calculation of the diffusion rate along a layer has been given by Chirikov⁴, and Tennyson et al.⁵, and Lieberman⁶ for the case of three resonances. For coupling among many resonances, a rigorous upper bound on the diffusion rate has been obtained by Nekhoroshev⁷, but this bound generally overestimates the rate by many orders of magnitude. A statistical treatment of the diffusion regime in which many resonances are important is under development^{4,10,11}, and some recent results will be described. Extensive numerical simulations of Arnold diffusion have been carried out^{4,8,11-13} and are summarized in the review article by Chirikov⁴.

Billiards problem--A simple example of a system illustrating Arnold diffusion is that of a ball bouncing back and forth between a

smooth wall at $z = h$ and a fixed wall at $z = 0$ which is rippled in two dimensions, x and y . The surface of section is given in terms of the ball positions in the x_n and y_n directions and the trajectory angles $\alpha_n = \tan^{-1} v_x/v_z$ and $\beta_n = \tan^{-1} v_y/v_z$, just before the n th collision with the rippled wall. The ball motion is shown schematically in Fig. 10, and the definitions of the variables in the x, z plane shown in Fig. 11. Assuming that the ripple is small, the rippled wall may be replaced by a flat wall at $z = 0$ whose normal vector is a function of x and y , analogous to the idea of a Fresnel mirror. The simplified difference equations exhibit the general features of the exact equations and may be written in explicit form

$$\begin{aligned}
 \alpha_{n+1} &= \alpha_n - 2 a_x k_x \sin k_x x + \mu k_x \gamma_c \\
 x_{n+1} &= x_n + 2 h \tan \alpha_{n+1} \\
 \beta_{n+1} &= \beta_n - 2 a_y k_y \sin k_y y + \mu k_y \gamma_c \\
 y_{n+1} &= y_n + 2 h \tan \beta_{n+1}
 \end{aligned}
 \tag{10}$$

where $\gamma_c = \sin(k_x x + k_y y)$, a_x and a_y are the amplitudes of the ripple in the x and y directions respectively, and μ is the amplitude of the diagonal ripple and represents the coupling between the x and y motions. A similar set of equations was examined numerically in pioneering studies by Froeschle¹⁰ and Froeschle and Scheidecker¹¹.

If $\mu = 0$, the system breaks into two uncoupled parts describing motion in x - z and y - z separately. Figure 12 shows the motion in the α - x surface of section for the uncoupled case. A number of different orbits are shown, each with different initial conditions. Each particle was run for 1000 iterations. The plot displays the usual features of a system with two degrees of freedom: (1) regular (KAM) orbits

(2) resonance islands and (3) stochastic orbits. The islands are examples of "higher order" regular (KAM) orbits. The central resonance at $\alpha = 0, x = 0$ corresponds to a stable motion for which the ball bounces up and down along z in the valley of the rippled wall. The islands encircling this resonance correspond to "adiabatic" motion in the valley with a small oscillation back and forth in x occurring over many bounce times in z . There are two major stochastic orbits visible in Fig. 12. The thick stochastic layers for α near $\pm\pi/2$ are regions of stochasticity produced by all overlapping resonances with one bounce period in z equal to one or more periods along x . Physically, these motions correspond to grazing angle trajectories, as shown in Fig. 12. Isolated from the thick layer by KAM curves spanning the space in x is the thin stochastic layer which has formed near the separatrix associated with the central resonance. Physically, as shown in Fig. 12, the separatrix orbit corresponds to a motion in x for which the ball is either just reflected or is just transmitted over a hill. The chaotic motion in this separatrix layer induces an Arnold diffusion in the coupled system, which appears as a diffusion in α along the separatrix layer of the β - y motion.

Coupled motion--A typical numerical calculation showing Arnold diffusion in the coupled system is given in Fig. 13. The surface of section for the system is 4-dimensional (α, x, β, y) , which we represent in the form of two, 2-dimensional plots (α, x) and (β, y) . Thus, two points, one in (α, x) and one in (β, y) , are required to specify a point in the 4-dimensional section. In Fig. 13, the two plots are superimposed for convenience, and x and y have been normalized to their respective wavelengths $2\pi/k_x$ and $2\pi/k_y$.

The initial condition as shown in Fig. 13a, has been chosen on an island encircling the central resonance in x , and within the thin separatrix layer for y . This corresponds to an initial adiabatic motion in x , well-confined in the valley, while in y the motion just reaches or passes over a hill. We observe numerically that the y motion is confined to its separatrix layer until the x -motion reaches its own separatrix layer. The successive stages of the diffusion of the α - x motion are shown in Fig. 13b, c and d respectively. In the absence of coupling ($\mu = 0$), the motion in the α - x plane should be confined to a smooth closed curve encircling the central resonance. For a finite coupling, α and x diffuse slowly due to the small randomizing influence of the stochastic β - y motion. The α - x diffusion is the motion along the β - y stochastic layer; i.e., it is the Arnold diffusion. The diffusion is shown for 1.5×10^5 , 3.5×10^6 , and 10^7 iterations of the mapping. At this time the α - x motion has diffused out to its own thin separatrix layer. Continued iteration of the mapping shows that the trajectory point diffuses over the entire α - x plane. In particular, the change of direction from diffusion along the β - y separatrix layer to diffusion along the α - x separatrix layer, illustrated in Fig. 4, has been observed numerically. Similarly, the change of direction from diffusion along a separatrix layer to diffusion along a thick layer (see Fig. 12) has been observed. Figure 14 shows these effects in the (α, β) action space (for $x = y = 0$) for the single initial condition of Fig. 13, after 5×10^7 iterations of the mapping. The trajectory has wandered randomly along thin and thick layers in the action space, as shown, spending much of its time in the region of thick layers for both α - x and β - y motion. This corresponds physically to motion with grazing angles of incidence in both the x and y directions.

All of this, however, is just part of the story. For recall that there exists a dense set of resonance surfaces in the action space. In particular, consider a coupling resonance, where physically the motion is "adiabatically" confined to a valley in both the x and y directions as the ball rapidly bounces along z. The ball executes small amplitude oscillations in both the x and y directions. If the oscillation frequencies ω_x and ω_y satisfy

$$m_1\omega_x + m_2\omega_y = 0,$$

then we have a resonance with its stochastic separatrix layer, which is also a part of the Arnold web. Including only a single coupling resonance, we have the action space shown in Fig. 15.

We now see a remarkable character of the motion near this coupling resonance in the billiards system. For initial conditions such that the system is placed in the separatrix of the coupling resonance, and thus within the Arnold web, the billiard motion initially appears "to be stable", consisting of a fast bounce motion in z and slower, small amplitude oscillations in x and y; in fact, it seems that the motion "is adiabatically confined" to a small neighborhood near $x = y = 0$. However, this is not the case. After a sufficient time, the billiard can be found executing grazing angle motion in both the x and y directions. The manner in which the diffusion proceeds is illustrated in Fig. 15. The diffusion typically proceeds first along the coupling resonance, then along the thin layer in x or y, and finally along the corresponding thick layer. With very high probability, the billiard motion will rarely "become retrapped" in a valley. This follows because the overwhelming fraction of the Arnold web is comprised of the "thick stochastic layers", with a negligible (but dense!) fraction of the web in regions such as the coupling resonance,

where the motion "appears to be adiabatic". On the other hand, for nearby initial conditions not on the Arnold web, the motion will be eternally confined to a small neighborhood near $x = y = 0$. Singular behavior indeed!

Stochastic pump model--The theoretical calculation of Arnold diffusion was first performed by Chirikov⁴, and his collaborators. For the billiards problem, the diffusion has been calculated by Tennyson et al.⁵ and by Lieberman⁶. The basic theoretical procedure is to break the original three-freedom system into two, two-freedom systems which are successively solved. A decomposition is illustrated in Fig. 16, where in (a) we show the original system and the coupling among the three freedoms due to resonances, and in (b) we show the simplest decomposition, the three resonance, stochastic pump model. In this model, the guiding resonance, along which the Arnold diffusion proceeds, is associated with freedom 2. The coupling between freedoms 1 and 2, described by the Hamiltonian

$$H_{\text{across}}(I_1, I_2, \theta_1, \theta_2) = \text{const}, \quad (11)$$

generates the chaotic motion across the separatrix layer. The Arnold diffusion is then obtained from

$$H_{\text{along}}(I_2, I_3, \theta_2, \theta_3) = \text{const} \quad (12)$$

which describes the coupling between freedoms 2 and 3. The motions described by (11) and (12) are solved successively, with (11) first yielding the stochastic variations of $\theta_2(t)$ and $I_2(t)$ in the separatrix layer. These are inserted into (12) which is then solved to obtain the stochastic variation $I_3(t)$ describing the Arnold diffusion. For details of these calculations and comparison with numerical simulation for the billiards problem, see Tennyson et al.⁵ and Lieberman⁶.

Physically, the model of Fig. 16b represents a pumping of stochasticity from freedom 1 into freedom 3 via the guiding resonance of freedom 2, since as shown by (9), large chaotic excursions ΔI_1 and ΔI_2 occur while ΔI_3 remains confined to the separatrix layer of width $\epsilon^{1/2}$. We refer to the motion described by (11) as the "stochastic pump".

Many resonance regime--Calculations based on the three resonance model have been reasonably successful in predicting the Arnold diffusion rate which is actually observed numerically^{4,5}. However, in the limit of weak coupling among the freedoms, the combined effect of many noninteracting resonances is important, and the three resonance theory predicts diffusion rates which are much lower than those observed from numerical simulation. The many resonance regime is called the Nekhoroshev region⁷⁻⁹ after the Soviet mathematician who first derived a rigorous upper bound on the diffusion rate there. However, Nekhoroshev's upper bound is generally many orders of magnitude larger than the actual diffusion rate.

The many resonance region has been examined numerically,^{4,9,12} and some analytic estimates were made^{4,8,9} for a simple model of a coupling resonance in a Hamiltonian system. The Hamiltonian studied was⁹:

$$H = (1/2)(p_1^2 + p_2^2) + (1/4)(x_1^4 + x_2^4) - \mu x_1 x_2 - \epsilon x_1 f(t) \quad (13)$$

where the p's are the momenta, the x's are the positions, and

$$f(t) = \frac{\cos vt}{1-A \cos vt} = \sum_m \frac{2e^{-\sigma m}}{\sigma} \cos(mt)$$

where $\sigma = (1-A^2)^{1/2}$ measures the harmonic content of the driving term f. This Hamiltonian describes the motion of two nonlinear oscillators which are coupled quadratically with strength μ . Oscillator 1 is driven by

a periodic function of time f with strength ϵ . Figure 17 shows the resonance surfaces in the $\omega_2(I)$ vs. $\omega_1(I)$ frequency space.

The Arnold diffusion was calculated numerically for motion along the coupling resonance $\omega_1 = \omega_2$, shown as the 45° line in the figure. The resonances of the driving term $f(t)$ with oscillator 1,

$$m\nu = \omega_1,$$

are shown as the solid vertical lines. Numerical calculations of the normalized diffusion rate D at $\sigma = 0.1$, $\omega = 4.5\nu$, are plotted versus $\mu^{-1/2}$, where μ is the normalized coupling strength, in Fig. 18. The theoretical prediction of the three resonance theory

$$D \propto \exp[-\mu^{1/2}]$$

is shown as the dashed straight line, for the three resonances

$$\omega_1 - \omega_2 = 0$$

$$4\nu - \omega_1 = 0$$

$$5\nu - \omega_1 = 0.$$

It can be seen that there is strong deviation from the three resonance theory for weak coupling strengths $\mu \rightarrow 0$. Also shown in the figure is Nekhoroshev's upper bound on the diffusion rate, for which

$$D_{\text{upper}} \propto \exp[-\mu^{-1/9}].$$

The discrepancy at small μ is resolved if we consider the harmonic resonances

$$m\nu - k\omega_1 = 0$$

between the driving term f and the driven oscillator 1. These resonances, shown as dashed vertical lines in Fig. 17, are excited with small amplitudes, and thus have very thin chaotic separatrix layers.

Nevertheless they strongly contribute to the overall Arnold diffusion because they lie close to the initial condition $4.5\nu = \omega_1$.

Theoretical calculation of the Arnold diffusion in the many resonance regime has been described by Chirikov^{4,8} and Chirikov et al.⁹. The theory is based on summing the non-phase correlated contributions of an infinite set of non-overlapping resonances, as shown in Fig. 16c. The theory is not well developed but yields results which are qualitatively in agreement with numerical calculations.

4. MODULATIONAL DIFFUSION

We turn now to another phenomena involving chaotic motion along resonance surfaces--the modulational diffusion. This mechanism is similar to Arnold diffusion, but as shown in Fig. 9, the chaotic motion is driven along a layer of overlapping resonances in the system. Due to the strong stochasticity in the overlapping layer, modulational diffusion is generally much stronger than Arnold diffusion. However, modulational diffusion is not universal. There is generally a resonance overlap condition for formation of the stochastic layer. Below this threshold, one sees only the weaker Arnold diffusion.

Modulational diffusion generally appears when the frequency in one freedom is slow compared to the frequencies in the other freedoms. Following Chirikov et al.⁹, we illustrate this for the example of the nonlinear coupled oscillators with Hamiltonian (13), but where the driving term is now

$$f(t) = \sum_m f_m \cos[m\nu t + \lambda \sin \Omega t]. \quad (14)$$

Thus, oscillator 1 is driven at harmonics of the frequency ν and is phase modulated with amplitude λ at the slow modulation frequency Ω .

Expanding (14) in a Fourier series yields

$$f(t) = \sum_{m,n} f_m J_n(\lambda) \cos[(m\nu + n\Omega)t].$$

The Bessel functions J_n have significant amplitude provided $n \lesssim \lambda$. The result is the formation of a multiplet layer of driving resonances of width approximately $2\Omega\lambda$ centered about each harmonic $m\nu$ of the driving frequency. The multiplets are shown as the vertical sets of lines in the $\omega_2 - \omega_1$ frequency space in Fig. 19. The modulational diffusion will appear as a chaotic motion along a set of overlapping resonances within a multiplet, in the vertical direction in Fig. 19. The motion along the overlapping multiplet layer is driven by the coupling resonance $\omega_1 = \omega_2$. This picture of modulational diffusion is illustrated in Fig. 16d.

Formation of multiplet layer--Near each multiplet

$$\omega_1(I_1) = m\nu$$

the motion can be described by the Hamiltonian.

$$H_1 = \frac{(\Delta I_1)^2}{2} + \epsilon \cos[\theta_1 + \lambda \sin \Omega t].$$

Physically this describes the motion of a ball in a one dimensional potential well

$$V(\theta_1, t) = \epsilon \cos[\theta_1 + \lambda \sin \Omega t]$$

which is slowly shaken back and forth with large amplitude, low frequency oscillations (see Fig. 20).

The conditions for a strong stochastic modulational layer are

(1) many resonances in a multiplet

$$\tau \gg 1$$

(2) adjacent multiplet layers do not overlap

$$v/\Omega \gg \lambda;$$

(3) resonances overlap within a multiplet layer

$$\epsilon > \sqrt{\lambda} \Omega^2/23.$$

The latter condition is derived using the usual resonance overlap criterion⁴ that the Chirikov stochasticity parameter $K = 1$. As the modulation frequency Ω is varied, we find the three regimes illustrated in Fig. 21.

At high frequencies Ω , for which (3) is not satisfied, multiplet resonances do not overlap and we have only the possibility of Arnold diffusion. At intermediate frequencies satisfying both (2) and (3), a thick chaotic layer is formed and we have strong modulational diffusion. At very low frequencies we enter the trapping regime. The overlapping separatrix layers merge and trapping of the ball in a valley of the potential $V(\theta_1)$ can occur (see Fig. 20). The modulational diffusion is weak in this regime.

These three regimes were first described by Tennyson¹⁴ in connection with a simple model of the beam-beam effect for bunched proton beams in the ISABELLE storage ring at Brookhaven. Figure 22, after Tennyson, shows the diffusion coefficient for chaotic motion across the modulational layer as the modulation period $P_s = 2\pi/\Omega$ is increased. Figure 23 shows numerical calculations of the Poincare section for the vertical motion ($P_y = V/\omega_0$ vs. Y) of a bunched proton beam as the modulation period is increased. A single modulation resonance becomes visible at $P_s = 200$ and a thick modulation layer has formed at $P_s = 600$.

Diffusion along the layer--We consider now chaotic motion along the overlapping resonance, which is the modulational diffusion. For

$$|\omega_2 - \omega_1| \lesssim \lambda\Omega \quad (15)$$

the condition of exact resonance

$$\omega_2 - \omega_1 + n\Omega = 0; |n| \lesssim \lambda$$

is met within the layer, and we expect a strong diffusion along the layer. The diffusion rate along the resonance can easily be calculated (see Chirikov et al.¹³). A more subtle problem is the calculation of the diffusion rate when the exact resonance condition is not met. This problem has been considered by Chirikov et al.^{13,15} for the coupled nonlinear oscillator problem. Figure 24 shows numerical calculations of the normalized modulational diffusion coefficient D_R as the frequency separation $|\omega_2 - \omega_1|$ is varied over a range of parameters λ , Ω , and ϵ . We note the plateau region when (15) is satisfied and the exponential drop in the diffusion rate when the exact resonance condition is not met (see also Fig. 19). The shape of the curve (solid line) has been calculated from an analytic theory containing two empirically determined parameters. The sharp drop near the plateau edge and the apparent wavy oscillation in the exponential tail show that there are many interesting features to be further explored in understanding modulational diffusion.

5. RESONANCE STREAMING

As a last example of chaotic motion along resonance surfaces we consider the process of resonance streaming^{16,18}. Streaming occurs in near-integrable systems that are subject to an externally generated transport process such as a diffusion or dissipation on the action space. In the absence of the external process, we have seen that a perturbed Hamiltonian system undergoes a motion which is a small bounded oscillation in the action space of the unperturbed system (see Fig. 2).

Although the oscillation itself may be unimportant, it necessitates an averaging procedure when the long term behavior is of interest. Specifically, transport phenomena must be described in terms of the motion of the oscillation-center, rather than of the instantaneous position. When the phase point is outside nonlinear resonance, the oscillation-center transport is almost identical to the unperturbed classical transport. But when the system is resonant, the two can be drastically different in both magnitude and direction. The difference is most pronounced when the resonance vector \mathbf{m}_k is nearly tangent to the resonance surface. In this case the oscillation-center can move rapidly along the resonance surface at a rate that is much greater than, but still proportional to, the classical transport rate.

Resonance streaming should not be confused with enhanced classical diffusion due to transport across resonance layers. This process is illustrated in Fig. 25a, where a large step in the action I_2 results when an initially untrapped phase point becomes trapped at the bottom of the island, swept around to the top of the island, and then detrapped. If the external noise is not conservative; i.e., if it can change the total energy of the system, then it essentially introduces an additional freedom into the original system (see note 1). Enhanced diffusion across resonance layers may be present in systems with two or more freedoms (including the noise).

Resonance streaming is illustrated in Fig. 25b, which shows an orbit moving up and to the left along a resonance surface in the action space. Streaming can only occur in systems with three or more freedoms (including non-conservative noise as a freedom). As shown in Fig. 8, streaming occurs when an orbit becomes trapped inside a resonance tube.

To understand the process of resonance streaming, we consider a near integrable two degree of freedom system with unperturbed actions I_1 and I_2 , having a resonance layer with resonance vector \underline{m}_R in the action space, as shown in Fig. 26. The initial motion is an oscillation within the resonance layer in the direction \underline{m}_R , about the initial oscillation center shown in the figure. Consider now a sudden non-energy conserving displacement B to a final position within the layer. The final oscillation center is displaced along the layer a distance A . We note that

$$A = B \sin \phi \csc \theta, \quad (16)$$

and therefore A may be much larger than B if θ is small. Furthermore the oscillation center displacement is always along the resonance. Thus any sequence of displacements (due to noise) that does not take the system out of resonance will result in a net displacement of the oscillation-center along the resonance, and this net displacement may be much larger in magnitude than the sum of the classical displacements. For more than three freedoms, the direction of the streaming in the resonance layer is given by the projection of the resonance vector \underline{m}_R onto the resonance surface.

A resonance layer may be classified into one of three distinct transport regimes for resonance streaming. These are approximately equivalent to the well known regimes of neoclassical theory¹⁹:

- 1) The oscillation-center (or weak transport) regime. For the oscillation-center concept to be valid, the system must remain in the resonance for a time greater than one oscillation period. This means that the oscillation period must be smaller than the time necessary for the classical transport process to move the

phase point from the center of the resonance to its edge. The enhancement ratio (16) is only valid in the oscillation-center regime.

- 2) The classical (or strong transport) regime. If the external process induces a motion that is faster than that induced by the resonance, then the presence of the resonance is inconsequential. The transport is said to be "classical" in this case.
- 3) The plateau regime. Since the upper limit of 1) does not coincide with the lower limit of 2), there is an intermediate situation. Here the phase point is not in the resonance long enough to complete one oscillation cycle, but the oscillation motion that does occur moves the phase point along the resonance a distance greater than the resonance width.

Examples of resonance streaming--We describe briefly two examples of resonance streaming. We first consider the effect of an external dissipation on a near integrable Hamiltonian system

$$H = H_0 + \epsilon H.$$

with

$$H_0 = I_1^2 + I_2^2 \tag{17}$$

and

$$\epsilon H_1 = 10^{-5} \cos(\theta_1 - \theta_2). \tag{18}$$

This system has unperturbed frequencies

$$\omega_1 = 2I_1, \quad \omega_2 = 2I_2$$

and a resonance surface

$$\omega_1 - \omega_2 = 0$$

or

$$I_1 - I_2 = 0$$

in the action space. For the external process we take a dissipation in I_2 alone, of the form

$$\dot{I}_2 = -10^{-5} I_2. \quad (19)$$

The motion must ultimately be attracted to the line $I_2 = 0$, but may detour along the resonance en route to its ultimate destination.

Figure 27 shows two computer generated trajectories plotted in the action space. The first trajectory is initially nonresonant. It drifts down to the resonance, makes a small horizontal jump as it crosses, and then continues on. The second trajectory becomes trapped inside the resonance as it attempts to cross and its oscillation-center is consequently constrained to move along the resonance curve. The libration angle is about 22 degrees and the ratio of resonant to nonresonant drift speed is 2.55. The resonant libration is slowly damped by the dissipation and the phase point is drawn toward the center of the resonance (barely perceptible here).

A second example is described by the same Hamiltonian (17) and (18), but where the external process is a diffusion in the action I_2 . The diffusion is defined by a sequence of small random jumps occurring once each unit time interval;

$$\Delta I_2 = 6 \times 10^{-5} \sin(r_n),$$

where r_n is a random number between 0 and 2π . Figure 28 shows the trajectory of the oscillation center for a phase point which starts at the center of the resonance and diffuses slowly out. Initially the oscillation center diffuses almost horizontally along the resonance

urve. Intervals where the trajectory diffuses back and forth across the resonance (see Fig. 25a), can also be seen. Eventually the phase point leaves the resonance, and the oscillation center stops its horizontal motion and begins to diffuse vertically, following the classical displacements.

The theoretical calculation of resonance streaming has been given by Tennyson¹⁶. Resonance streaming effects may be important in high temperature plasma confinement experiments and in high energy particle storage rings.

6. CONCLUSION

For three or more freedoms, a new phenomenon appears in near integrable Hamiltonian systems, not present in systems with one or two freedoms: chaotic motion along resonance layers. Three mechanisms for such motion have been described: Arnold diffusion, modulational diffusion and resonance streaming. Table 1 summarizes some important properties of these mechanisms. There are probably many interesting effects to be discovered concerning chaotic motion in multidimensional systems.

Mechanism	Perturbation Strength	Driving source for stochastic pump	Driving source along resonance layer(s)
ARNOLD DIFFUSION	$\epsilon > 0$	ONE RESONANCE	ONE RESONANCE
	$\epsilon > 0$	MANY NON- OVERLAPPING RESONANCES (NEKHOROSHEV)	MANY NON- OVERLAPPING RESONANCES
MODULATIONAL DIFFUSION	$\epsilon > \epsilon_{\text{CRIT}}$	MANY OVERLAPPING RESONANCES	ONE RESONANCE
RESONANCE STREAMING	$\epsilon > 0$	ONE RESONANCE	EXTRINSIC DIFFUSION OR DISSIPATION "NOISE"

NOTES AND REFERENCES

1. A time varying Hamiltonian $H(p, q, t)$ with N p 's and q 's can be transformed to a time independent form with $N+1$ p 's and q 's by introducing an extended phase space, and is thus equivalent to a system with $N+1$ freedoms.
2. We generally consider "near-integrable" systems for which $H = H_0 + \epsilon H_1$, with H_0 integrable, H not integrable, and ϵ the perturbation strength.
3. Arnold, V. I., Dokl. Akad. Nauk SSSR 156, 9 (1964).
4. Chirikov, B. V., Phys. Reports 52, 5: 263-379 (1979).
5. Tennyson, J. L., M. A. Lieberman and A. J. Lichtenberg, American Institute of Physics Conf. Proc. 57 (1979).
6. Lieberman, M. A., Ann. N. Y. Acad. Sci. 357 (1980).
7. Nekhoroshev, N. N., Usp. Mat. Nauk USSR 32, 6 (1977).
8. Chirikov, B. V., Fizika Plasmy 4, 3: 521 (1978).
9. Chirikov, B. V., J. Ford and F. Vivaldi, American Institute of Physics Conf. Proc. 57 (1979).
10. Froeschle, C. Astrophys. Space Sci. 14, 110 (1971).
11. Froeschle, C. and J. P. Scheidecker, Astrophys. Space Sci. 25, 373 (1973).
12. Gadiyak, G. M., F. M. Izrailev, B. V. Chirikov, Proc. 7th Int'l. Conf. on Nonlinear Oscillations (Berlin, 1975), vol. II, 1:315.
13. Chirikov, B. V., F. M. Izrailev and D. L. Shepelyansky, "Dynamical Stochasticity in Classical Mechanics," Preprint 80-209, Institute of Nuclear Physics, Novosibirsk, USSR (1980).
14. Tennyson, J. L., American Institute of Physics Conf. Proc. 57 (1979).

15. Chirikov, B. V. and D. L. Shepelyansky, "Diffusion in the Presence of Many Overlapping Nonlinear Resonances," Preprint 80-211, Institute of Nuclear Physics, Novosibirsk, USSR (1980), in Russian.
16. Tennyson, J. L., "Enhancement of Classical Transport Processes Along Resonances in Near Integrable Systems with Many Degrees of Freedom," Electronics Research Lab., Memo. UCB/ERL M81/7, University of California, Berkeley, Ca. (25, Jan. 1981).
17. Tennyson, J., SLAC Pub. 2624 (1980).
18. Chirikov, B. V., Sov. J. Plasma Phys. 5, 492 (1979).
19. Galeev, A. A. and R. Z. Sagdeev, JETP 26, 233 (1968).

FIGURE CAPTIONS

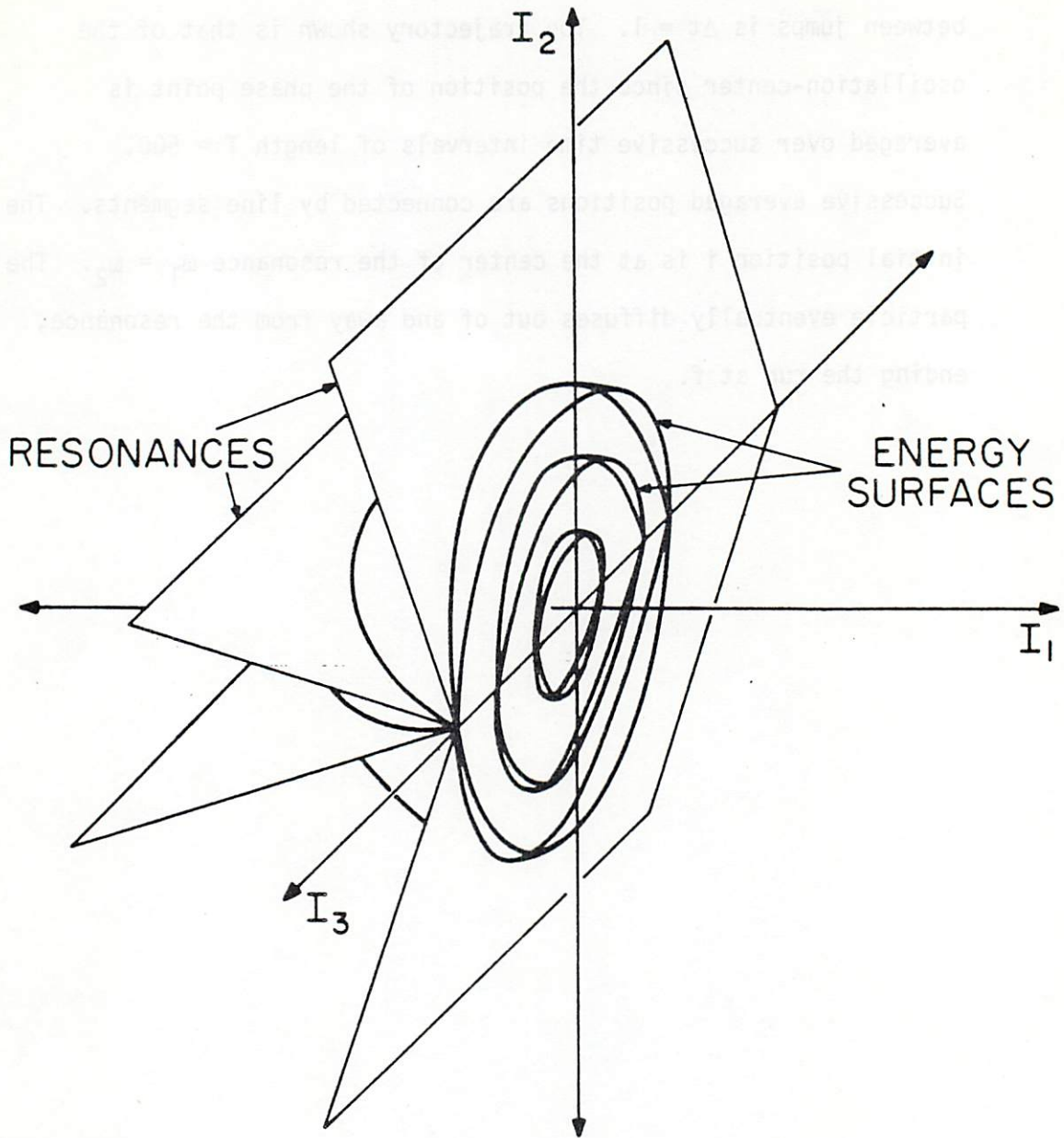
1. The action space, showing energy surfaces and resonance surfaces for the unperturbed, free particle Hamiltonian.
2. The effect of non-resonant and resonant perturbations: (a) non-resonant perturbations m_k drive oscillations of order ϵ . (b) A resonant perturbation m_R drives an oscillation along m_R of order $\epsilon^{1/2}$.
3. Resonance curves (lines) and energy contours (ellipses) in two dimensional action space. The Hamiltonian function for this example is $H_0(\underline{I}) = I_1^2 + (6I_2)^2$. The resonance labels are the values of m_1 where $\omega_1 m_1 + \omega_2 = 0$.
4. Intersection of two resonance surfaces in an action space having three freedoms. An energy conserving motion (wiggly line) from one resonance surface to another is possible.
5. The Arnold web for the free particle Hamiltonian. Only some of the intersecting resonances are shown.
6. Isolation of regions by KAM surfaces (lines). In (a) the plane is divided by lines into a set of closed areas; in (b) the volume is not divided by lines into a set of closed volumes.
7. Projection of a resonance layer in phase space onto the two-dimensional surface defined by the resonance action I_R and the resonance phase angle ψ_R .
8. Three dimensional projection of a resonance layer in phase space. I_S denotes an action variable along the resonance layer. The regions in which Arnold diffusion and resonance streaming take place are identified.
9. Three dimensional projection of a set of overlapping resonances in phase space. Modulational diffusion takes place along the layer as shown.

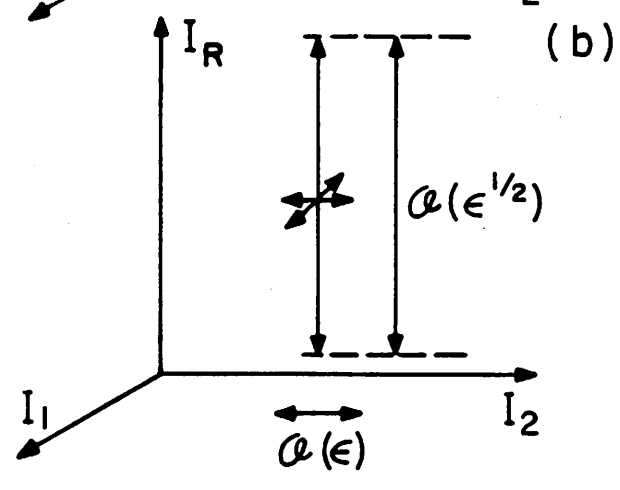
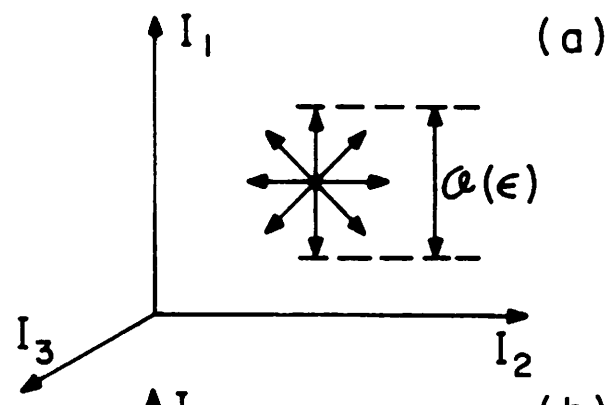
10. The three dimensional billiards problem. A point particle bounces back and forth between a smooth and a periodically rippled wall.
11. Motion in two degrees of freedom, illustrating the definition of the trajectory angle α_n , and the bounce position x_n just before the n^{th} collision with the rippled wall.
12. Motion in the α - x surface of section for the uncoupled billiards problem. The parameters are $\mu = 0$; $\lambda_x:h:a_x$ as 100:10:2; $\lambda_x = 2\pi/k_x$. Fifteen particles are started at $x = 0$ and allowed to run for 1000 iterations each.
13. Thin layer diffusion. Initial conditions are close to the central resonance in the α - x space and within the separatrix stochastic layer in the β - y space. Parameters are $\mu/h = .004$; $\lambda_x:h:a_x$ and $\lambda_y:h:a_y$ as 100:10:2.
14. Projection of motion in the α - β action space for $x \approx 0$, $y \approx 0$. The parameters and initial conditions are the same as for Fig. 13. After 5×10^7 iterations, the orbit has wandered in and out of the thick and thin layers of both the α - x and β - y motions.
15. Arnold diffusion in the three dimensional billiards problem, in the angle of incidence space α - β . The initial condition is chosen to be within the separatrix of motion associated with the coupling resonance $\omega_x = \omega_y$. The initial motion with near normal incidence diffuses towards motion with large angles of incidence. A typical diffusive path is sketched.
16. Decomposition of a three freedom system for the theoretical calculation of chaotic motion along a resonance layer. (a) original system with coupling among all degrees of freedom. (b) The three resonance, stochastic pump model for Arnold diffusion. (c) Model for Arnold diffusion in the many resonance (Nekhoroshev) regime. (d) Model for modulational diffusion.

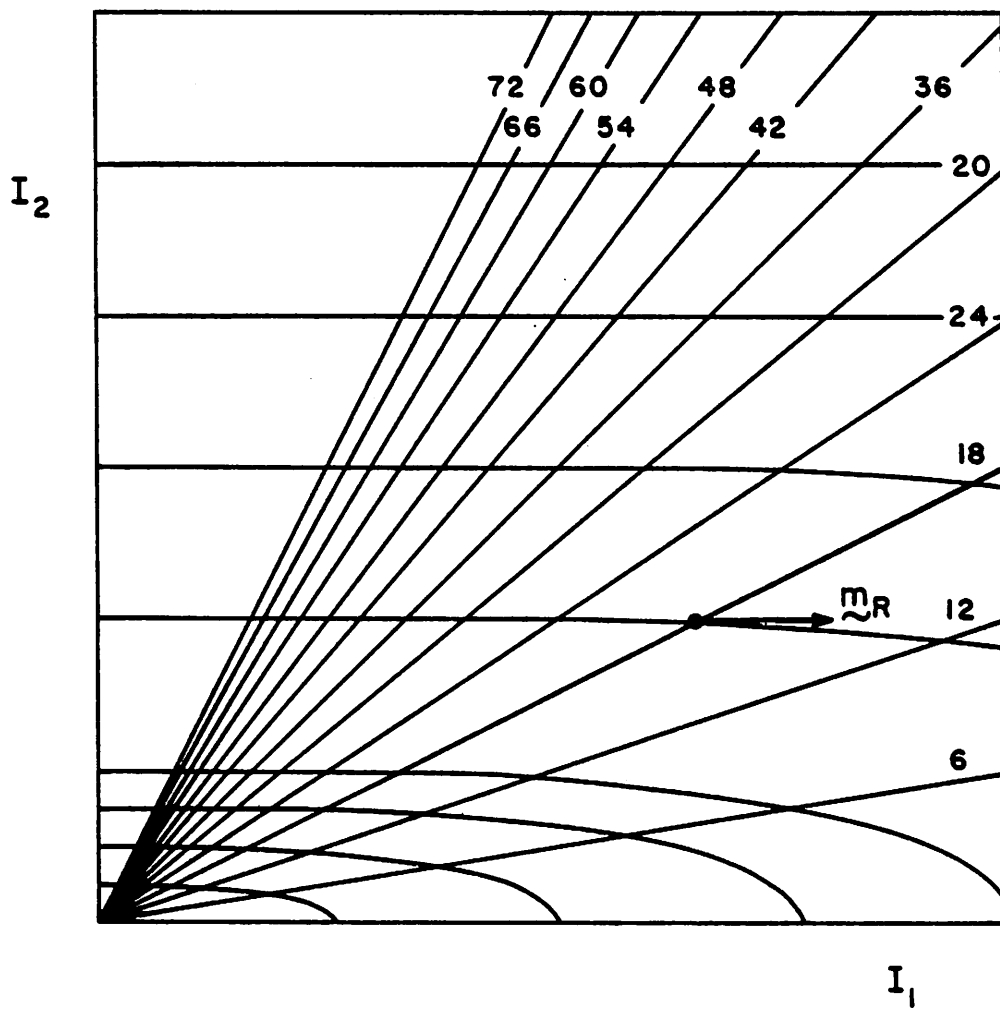
17. Resonances in the $\omega_2 - \omega_1$ frequency space for the Hamiltonian (13). The diagonal line shows the coupling resonance between oscillators 1 and 2. The solid vertical lines show the resonances of the driving term with oscillator 1. The Arnold diffusion has been calculated along the coupling resonance at the point shown (after Chirikov et al.⁹).
18. Normalized Arnold diffusion rate D versus $\mu^{-1/2}$, where μ is the normalized coupling strength. The dots are numerical calculations, the straight dashed line is the prediction of the three resonance theory, and Nekhoroshev's upper bound is also shown (after Chirikov et al.⁹).
19. Resonances in the $\omega_2 - \omega_1$ frequency space for the Hamiltonian (13) with modulational driving term (14) (after Chirikov et al.¹³). The coupling resonance is shown as the 45° line. The multiplets of resonances which form near harmonics of the driving frequency ν are shown as the sets of vertical lines. The modulational diffusion appears along a multiplet layer. The plateau and exponential tail regimes of the diffusion are indicated in the figure.
20. Model for the stochastic pump which generates the chaotic motion across the multiplet layer.
21. Three regimes in the formation of an overlapping layer of modulational resonances as the modulation frequency Ω is varied. (a) High Ω leads to non-overlapping resonances within the multiplet. There is Arnold diffusion but no modulational diffusion. (b) intermediate Ω leads to overlapping of modulational resonances and strong modulational diffusion. (c) Low Ω leads to formation of a trapping (regular) regime and weak modulational diffusion.

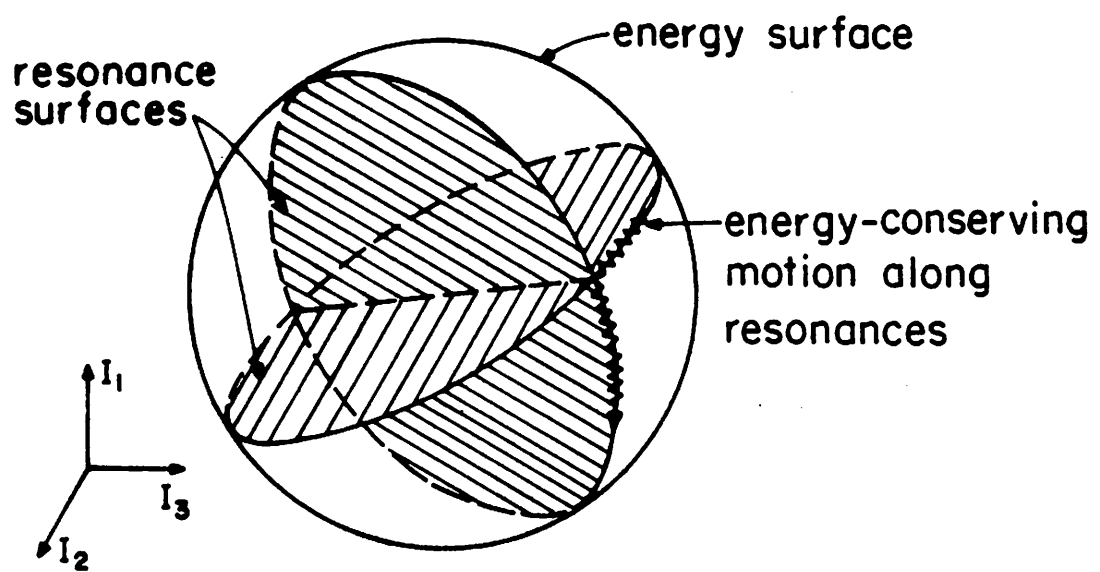
22. Behavior of the normalized diffusion coefficient describing chaotic motion across a modulational resonance layer (after Tennyson¹⁴).
23. Simulation of bunched proton-proton crossing beams in ISABELLE. The Poincare section ($P_Y = V/\omega_0$ vs. Y) for the vertical motion is shown as the modulation period $P_s = 2\pi/\Omega$ is increased. A modulational resonance layer is formed (after Tennyson¹⁴).
24. Normalized modulational diffusion coefficient D_R as the frequency separation $|\omega_2 - \omega_1|$ is varied. The points show numerical calculations over a wide range of values of λ , Ω and ϵ . The solid curve shows an analytical calculation containing two empirically determined parameters (after Chirikov et al.¹³).
25. Chaotic motion near resonance layers due to external noise or dissipative processes. (a) Enhanced transport across resonances
(b) Resonance streaming which is an enhanced transport along resonances.
26. Oscillation center displacement inside a resonance layer. The phase point, oscillating vertically, makes a jump B due to external noise or dissipation. The oscillation center makes a corresponding jump A. Note that A may be greater than B.
27. Dissipative streaming in two dimensions. Two trajectories are shown in action space. The first phase point begins at i_1 and descends to f_1 , crossing the coupling resonance $\omega_1 = \omega_2$ on its way. The second phase point descends from i_2 but instead of crossing the resonance, becomes trapped and thus streams along the resonance. The time intervals for the two trajectories are the same. The dashed lines show the energy contours at the initial and final positions.

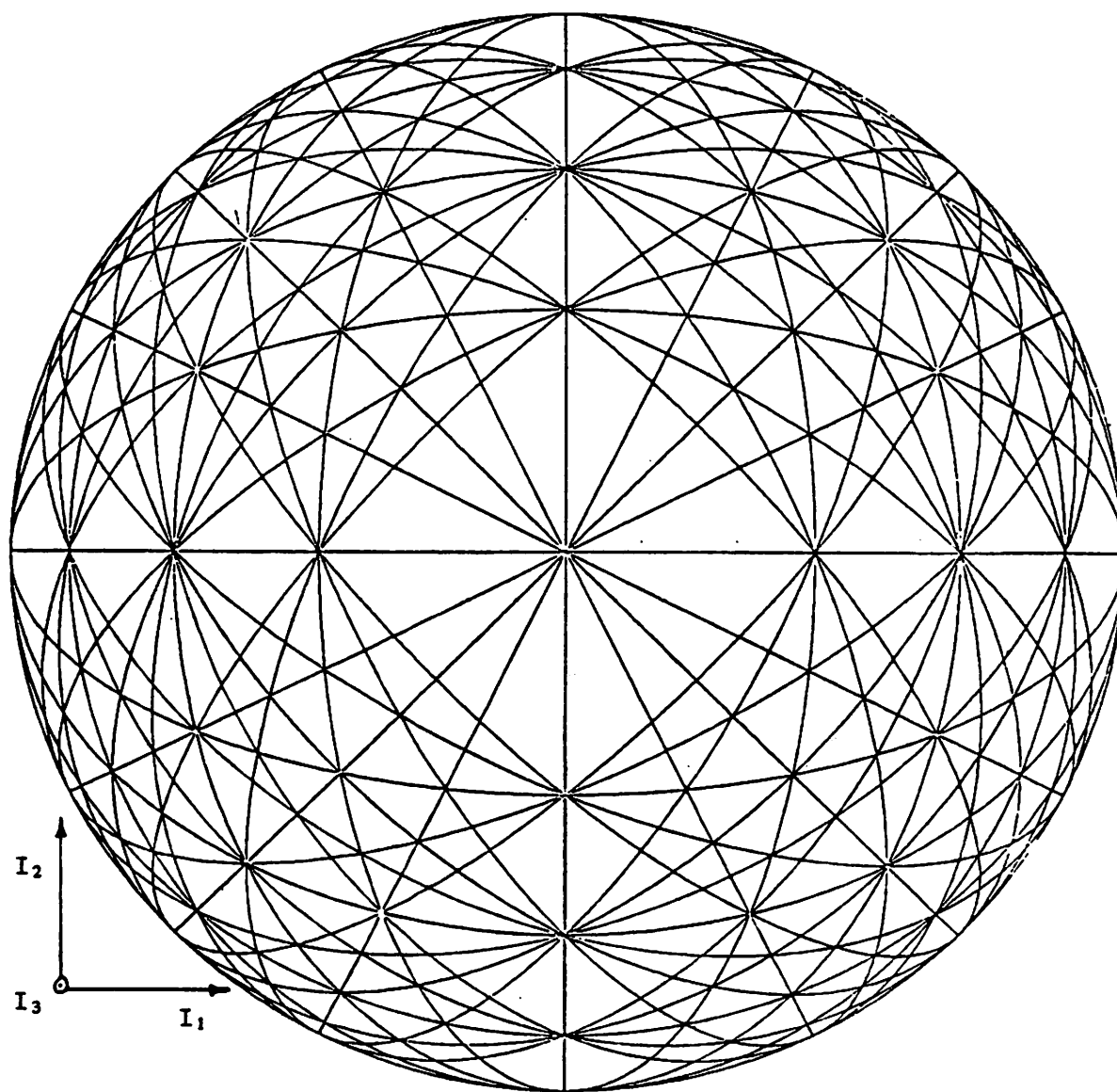
28. Resonance streaming in two dimensions due to diffusion. The Hamiltonian function is the same as in Fig. 27. The external process is now a vertical diffusion consisting of small steps in ΔI_2 , and the time between jumps is $\Delta t = 1$. The trajectory shown is that of the oscillation-center since the position of the phase point is averaged over successive time intervals of length $T = 500$. Successive averaged positions are connected by line segments. The initial position i is at the center of the resonance $\omega_1 = \omega_2$. The particle eventually diffuses out of and away from the resonance, ending the run at f .



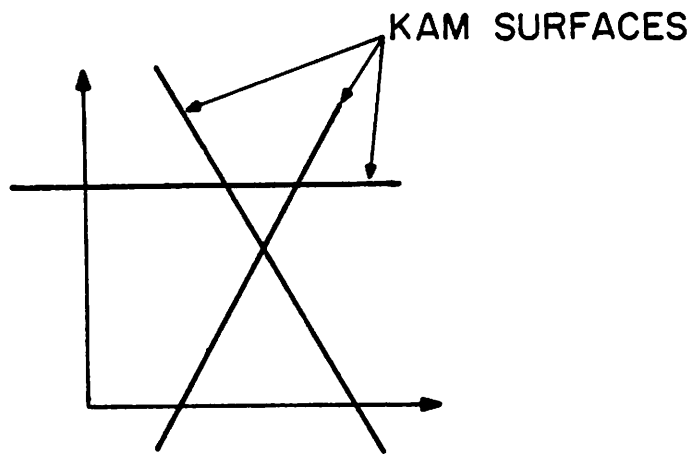




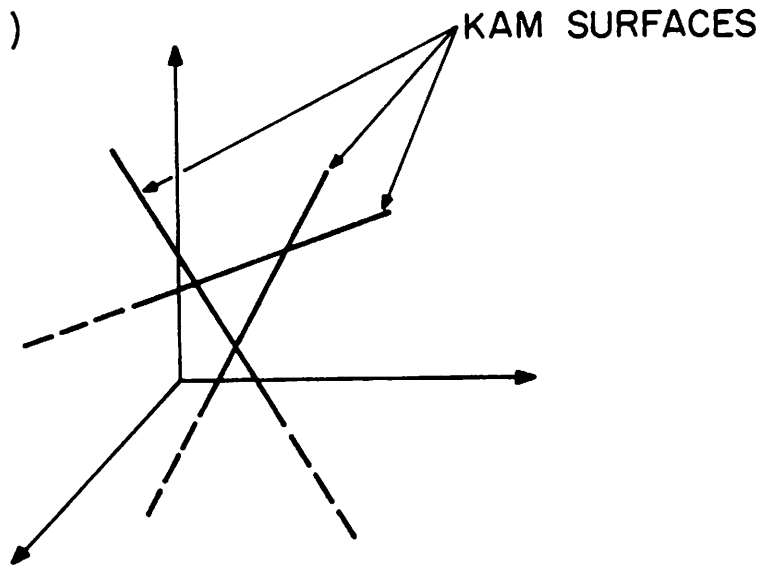


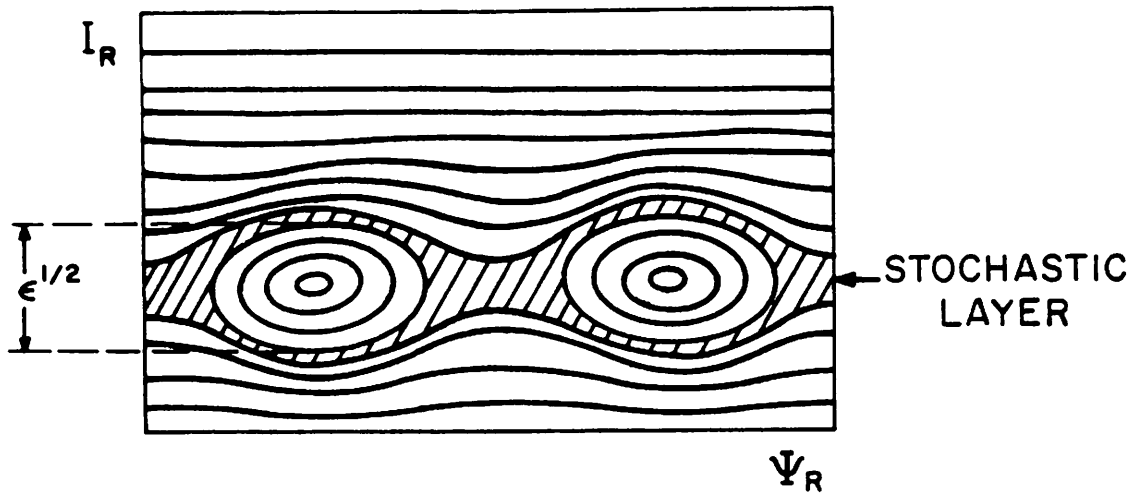


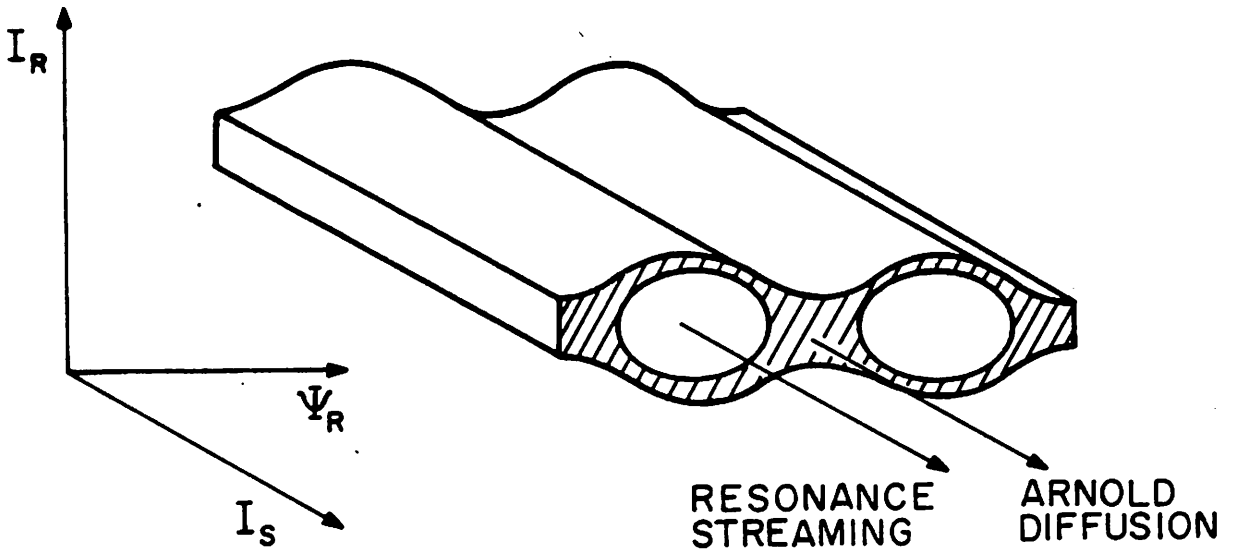
(a)

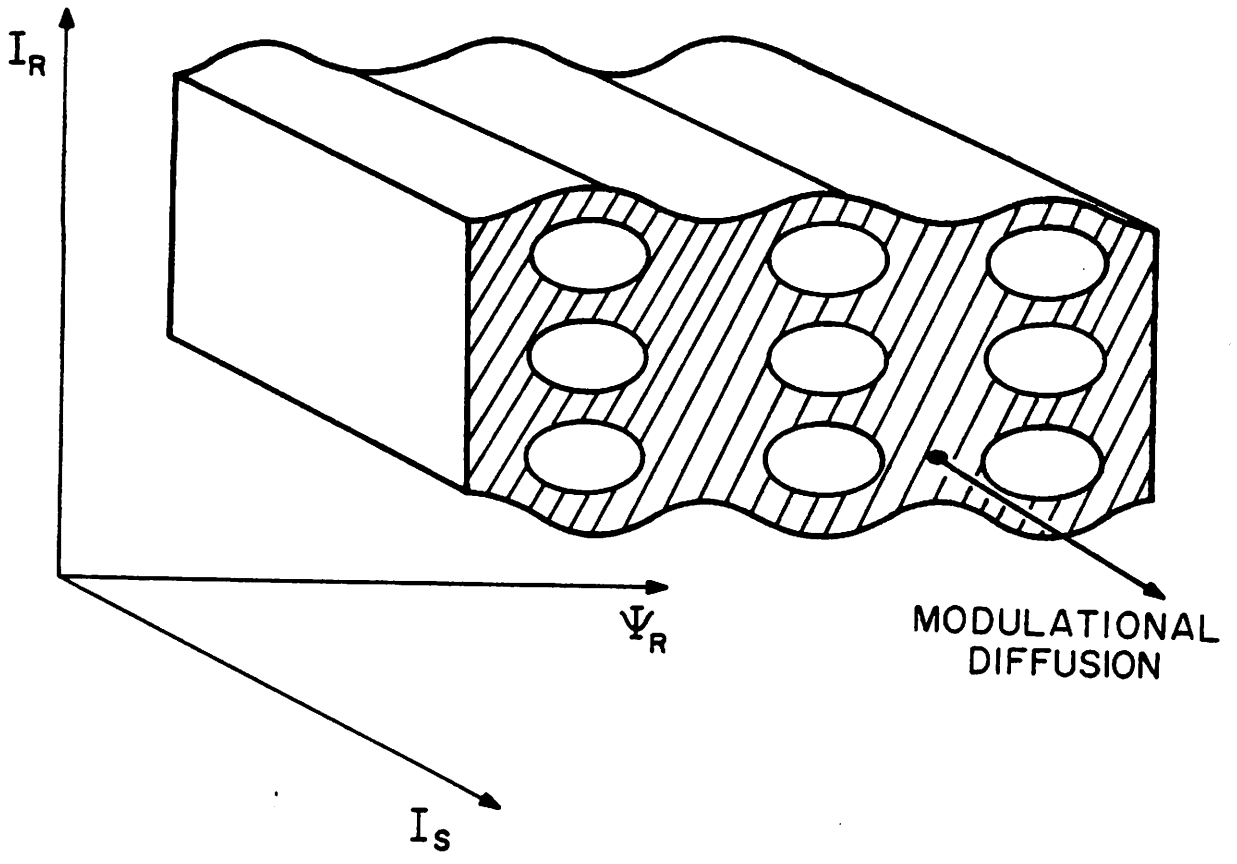


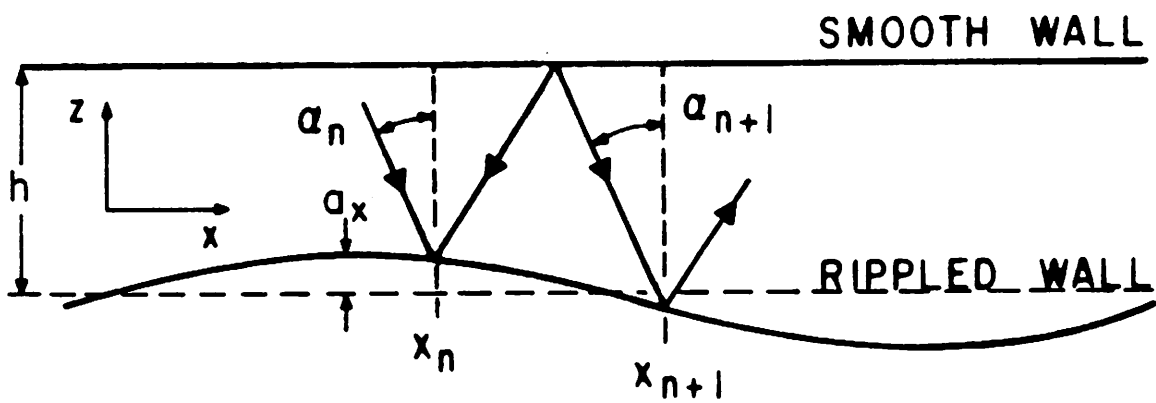
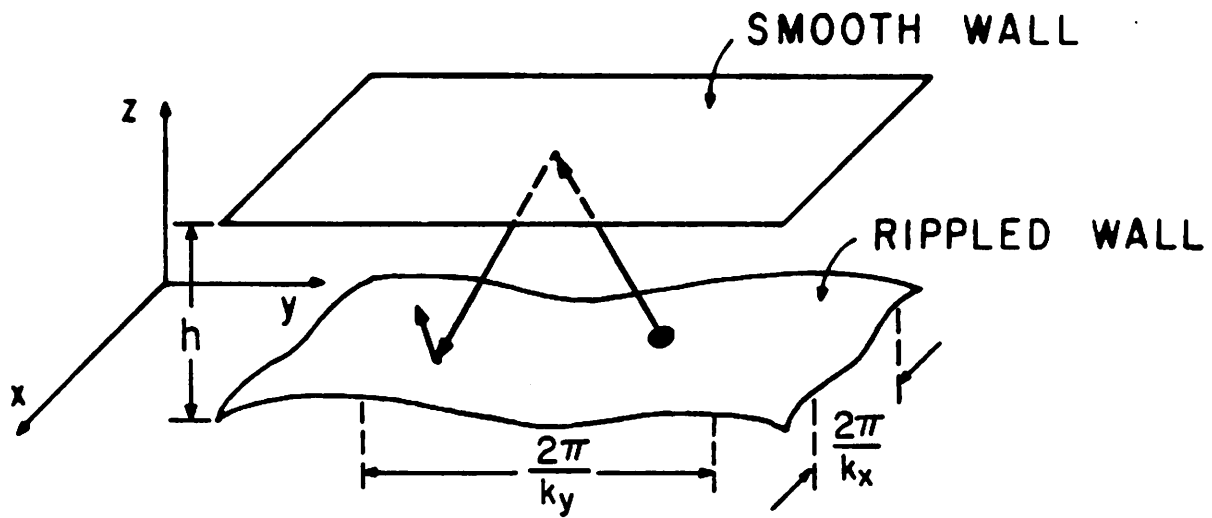
(b)

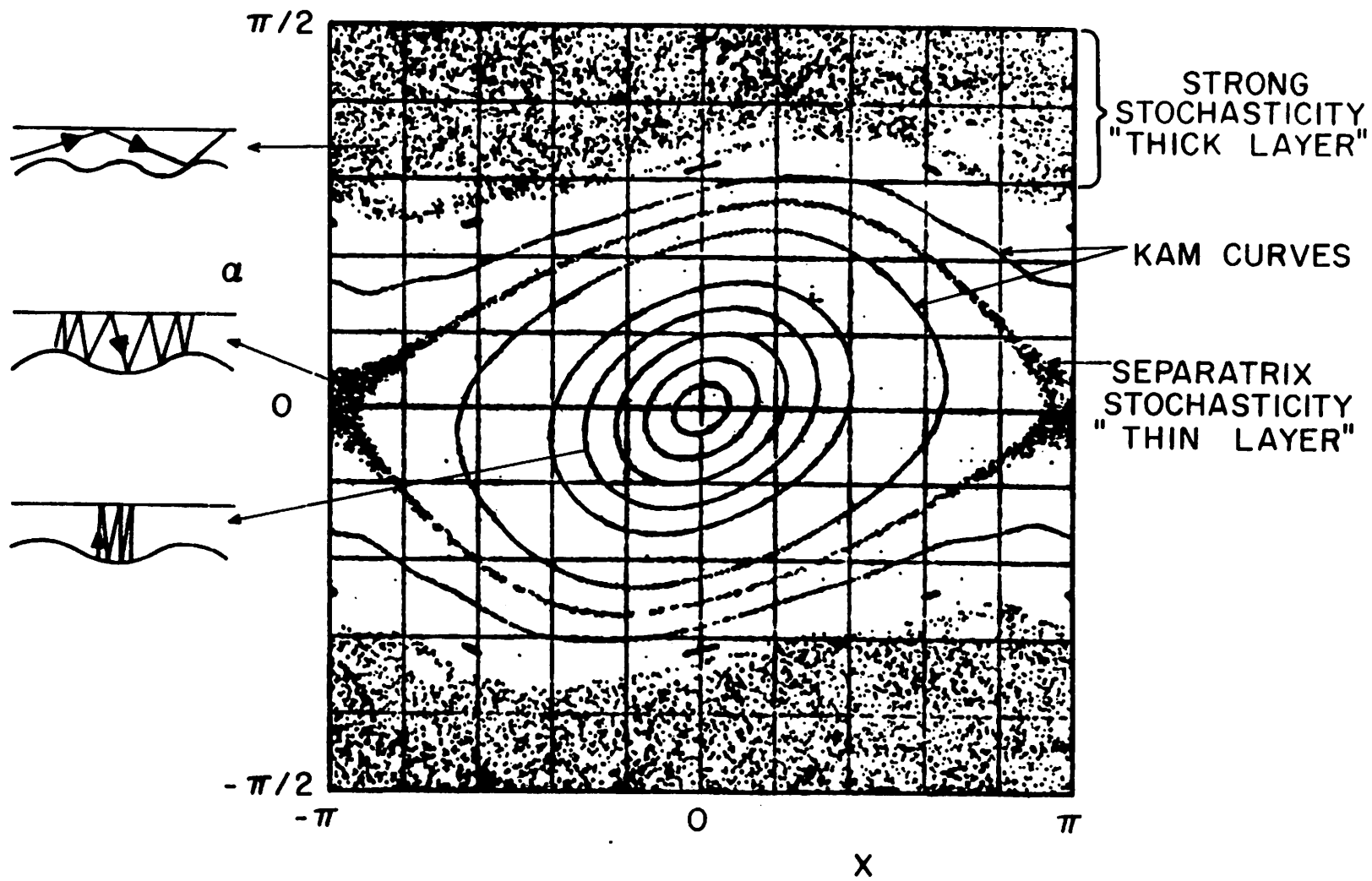


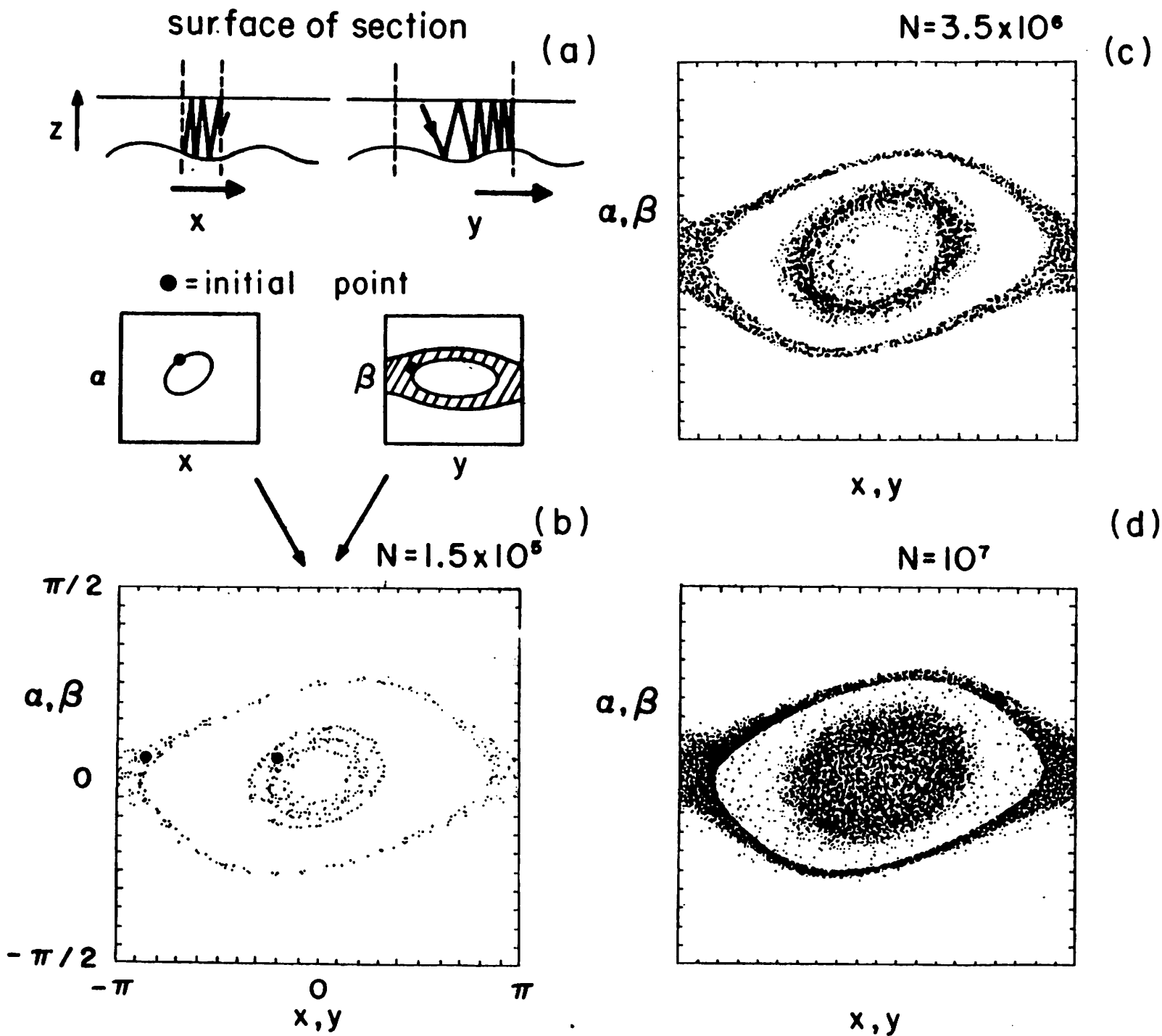




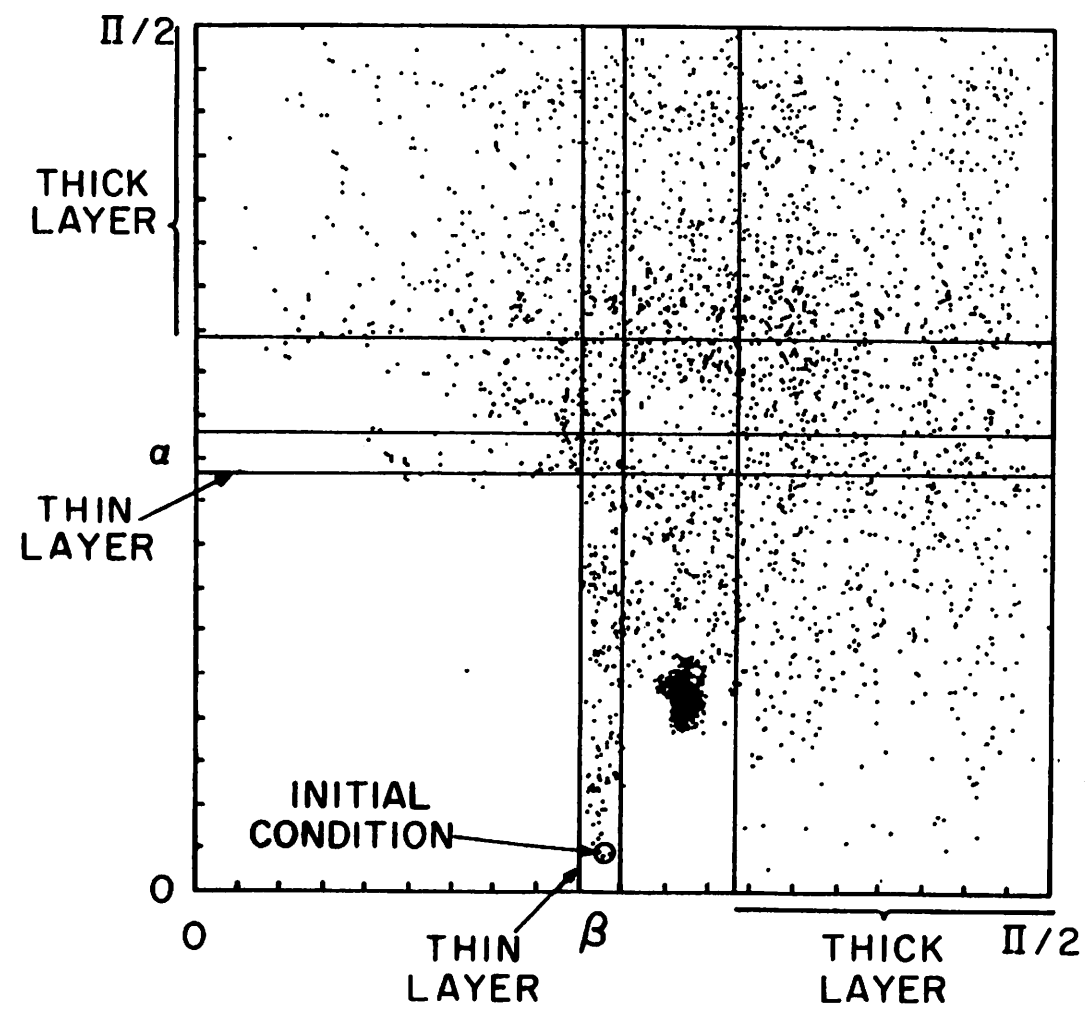


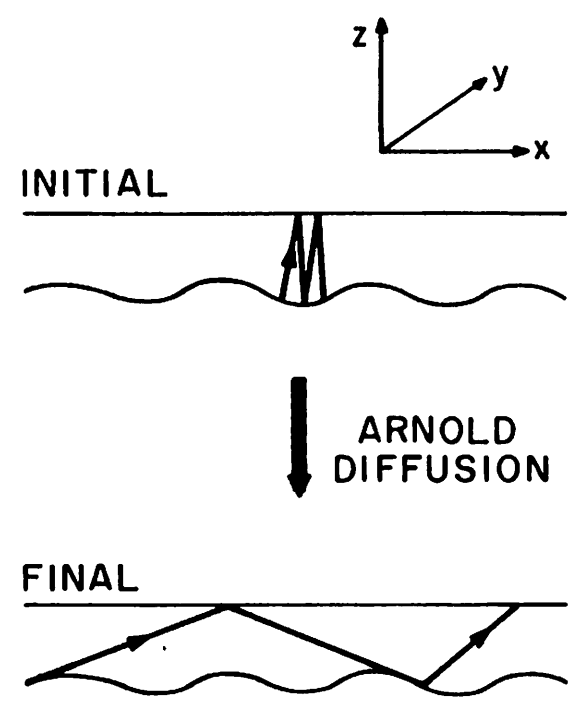
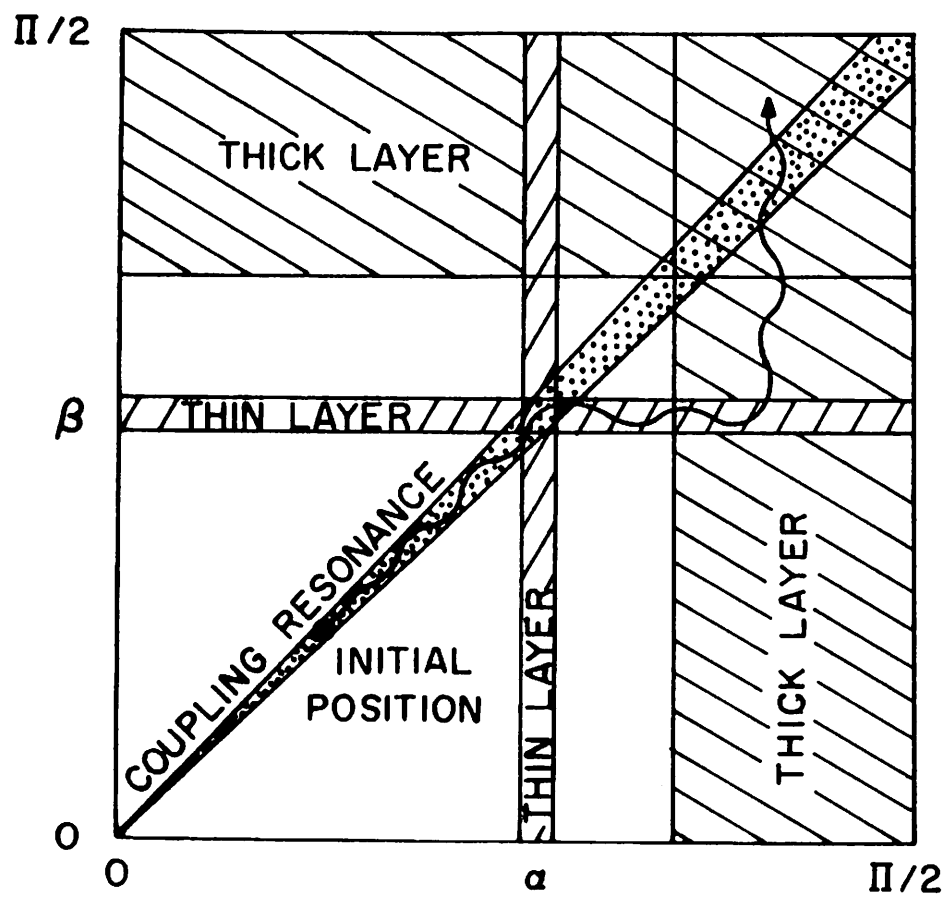


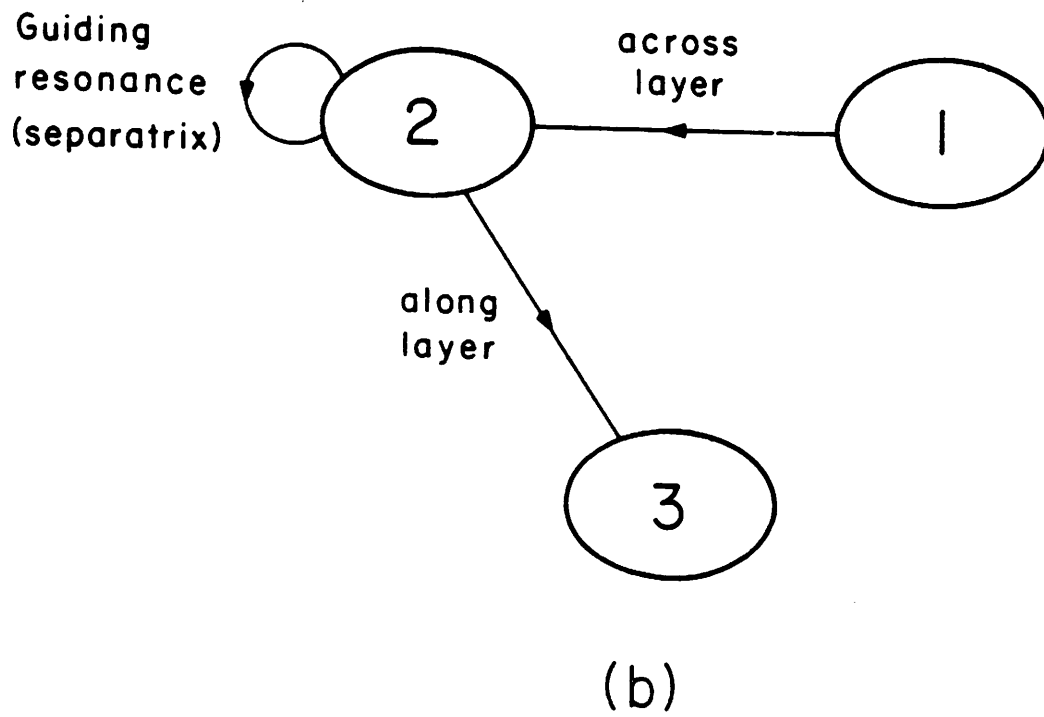
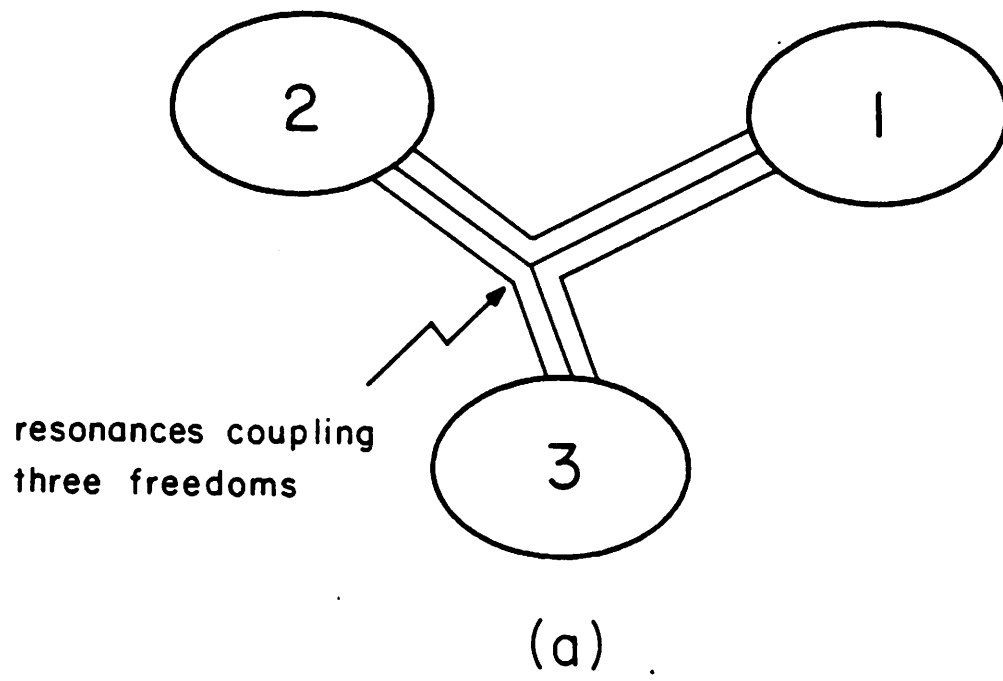


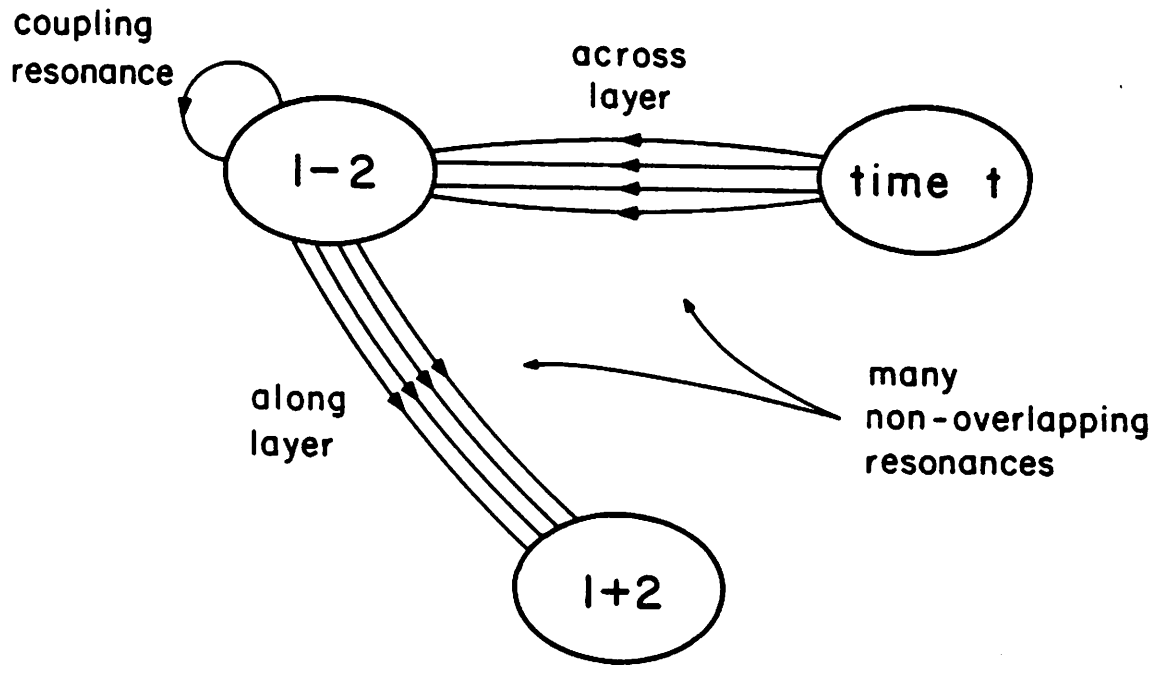


5×10^7

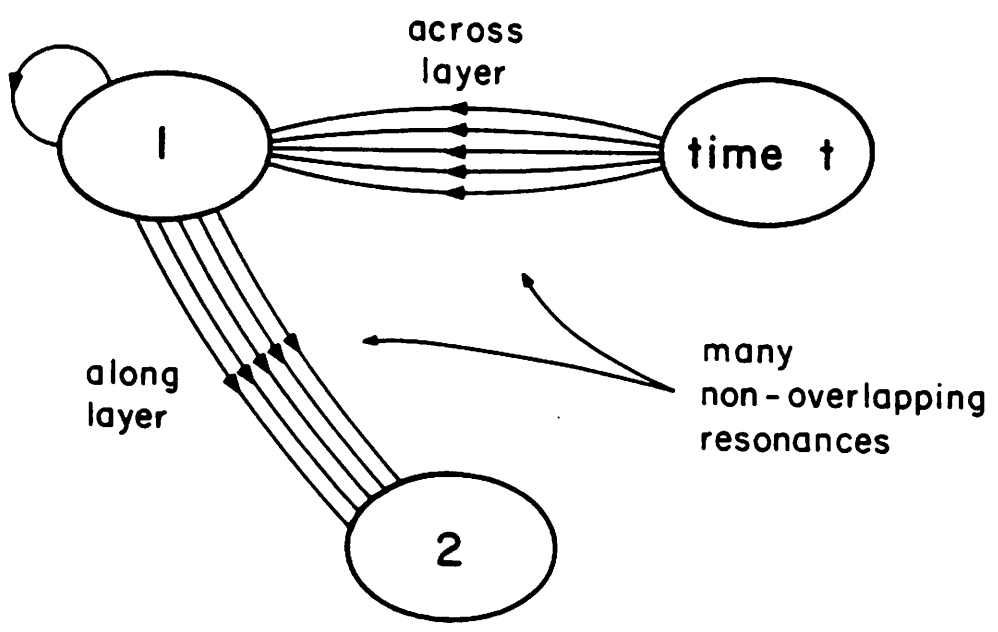




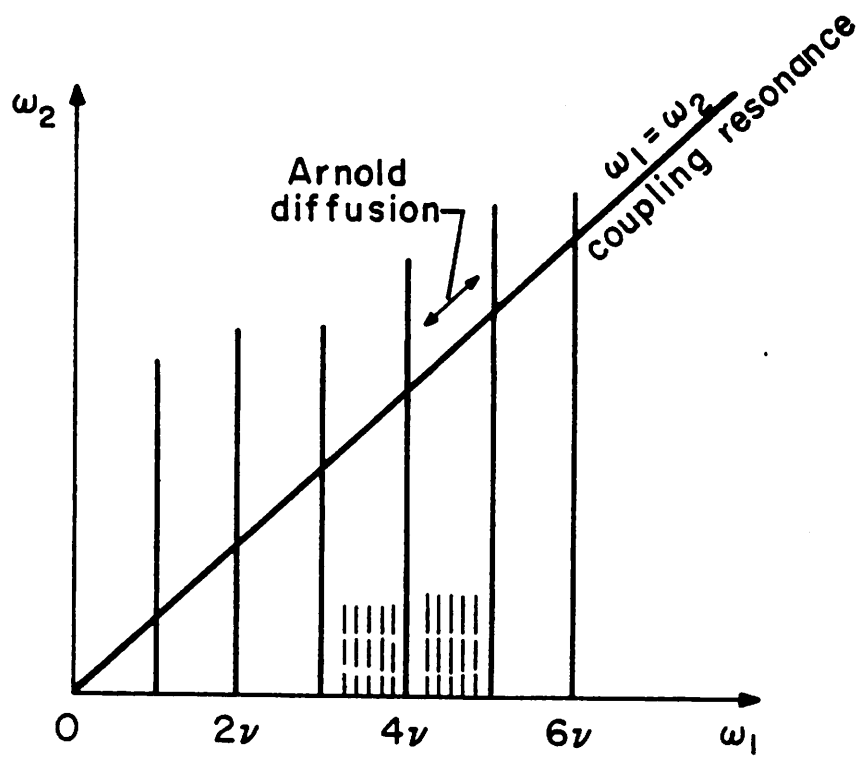


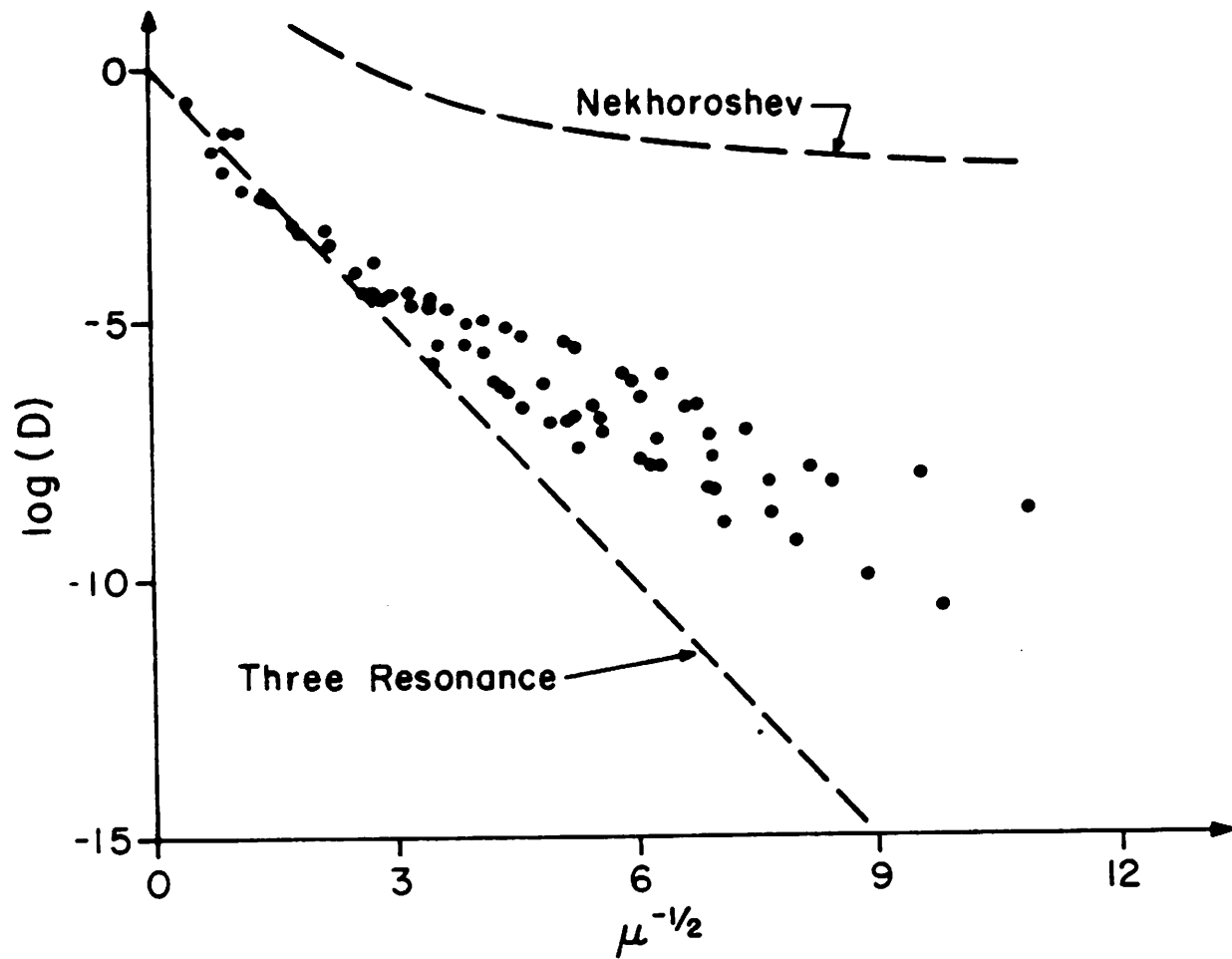


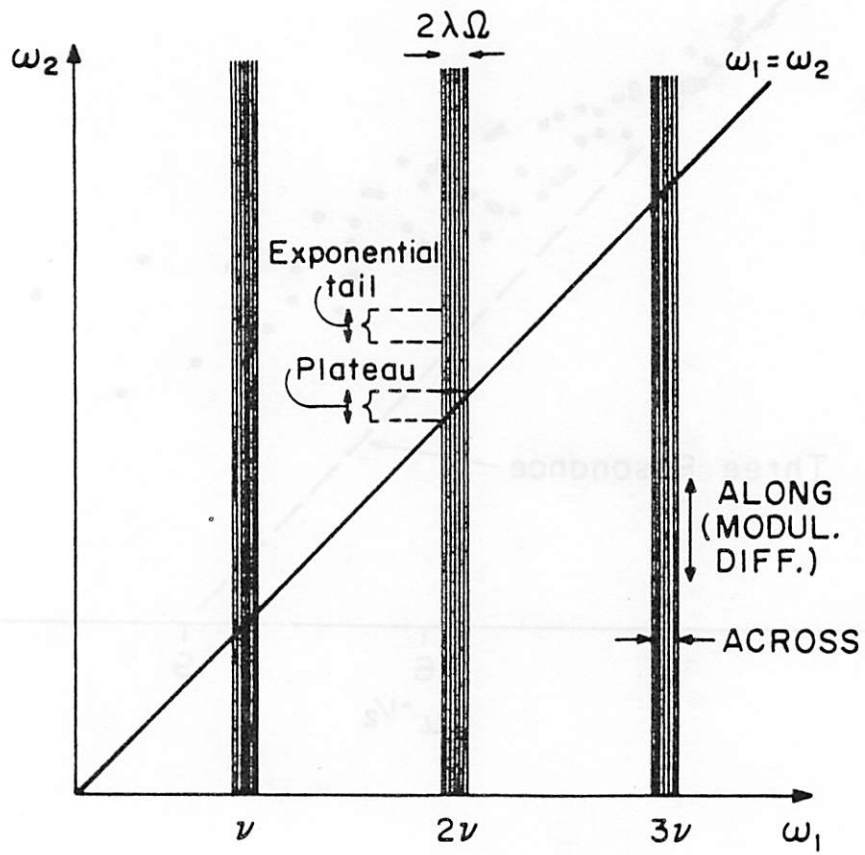
(c)

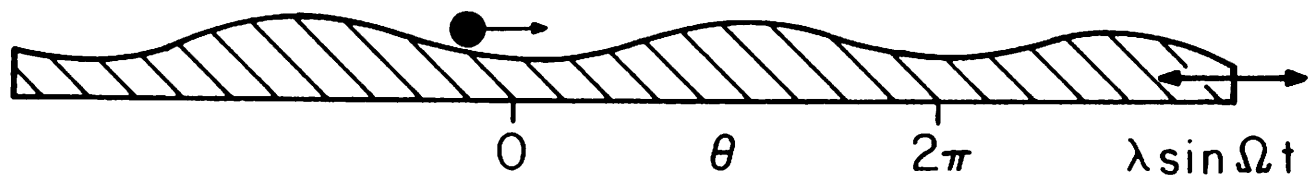


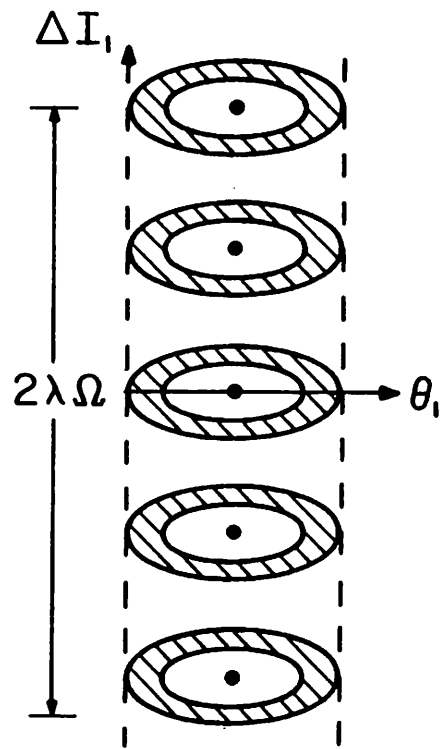
(d)



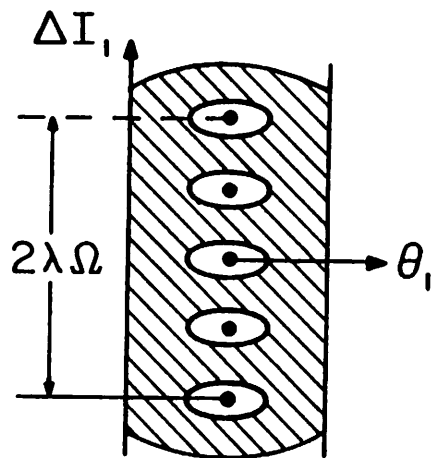




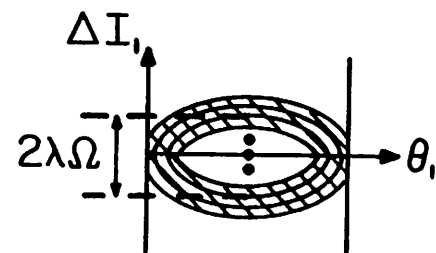




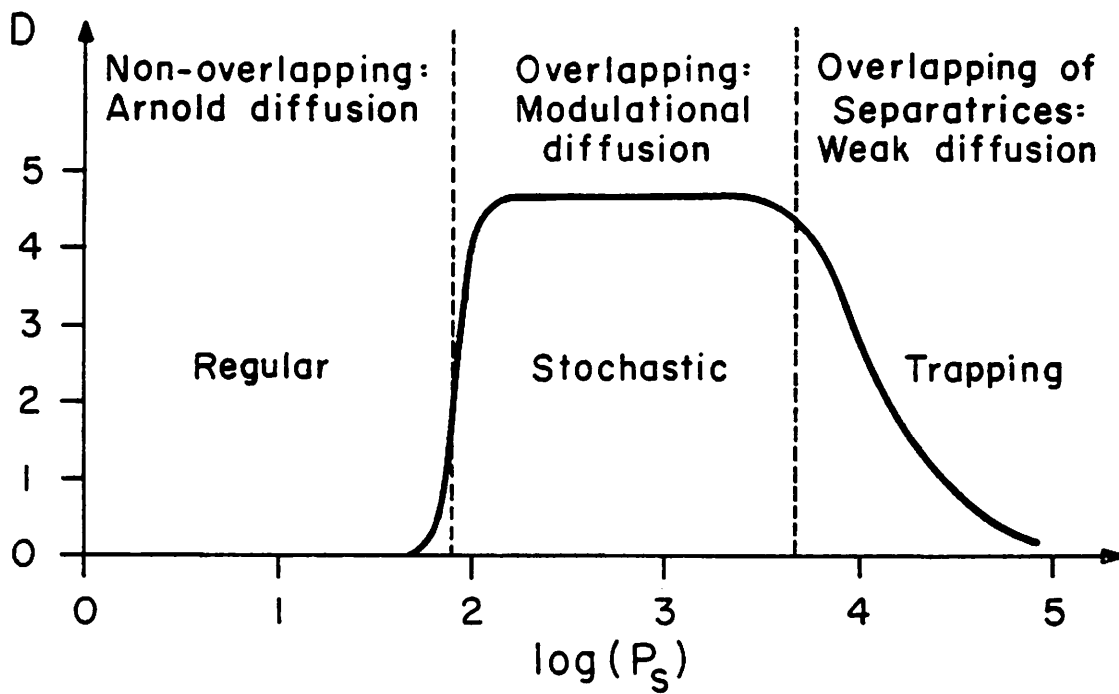
(a)



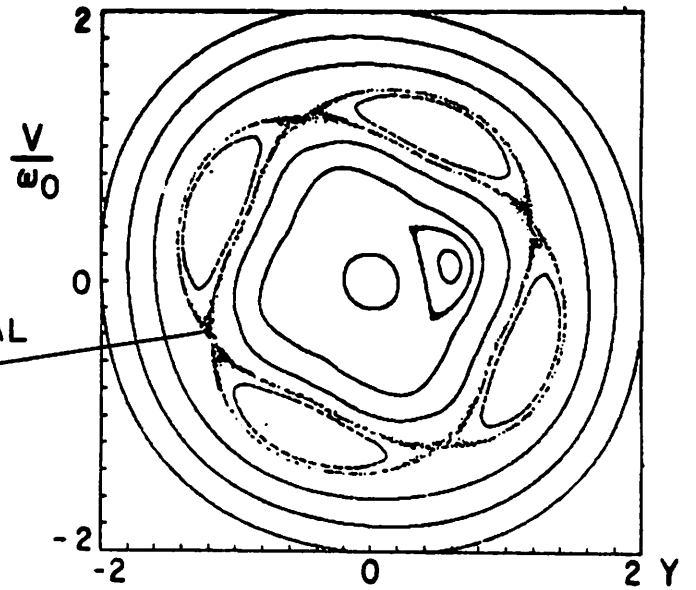
(b)



(c)

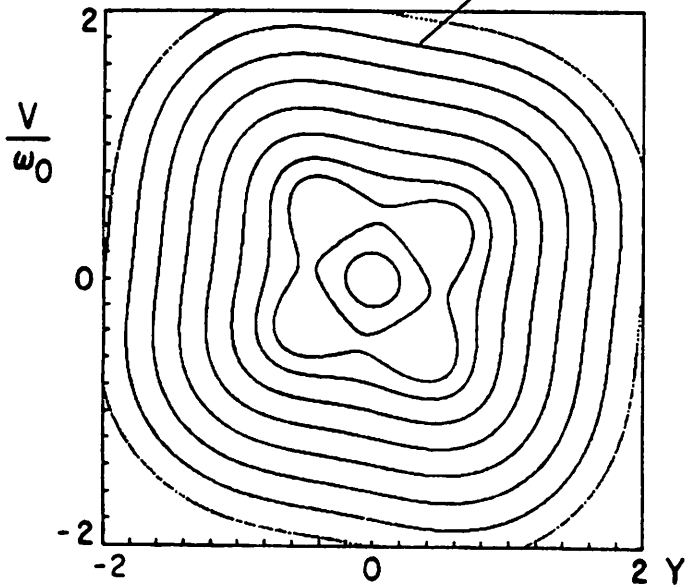


A SINGLE
MODULATIONAL
RESONANCE

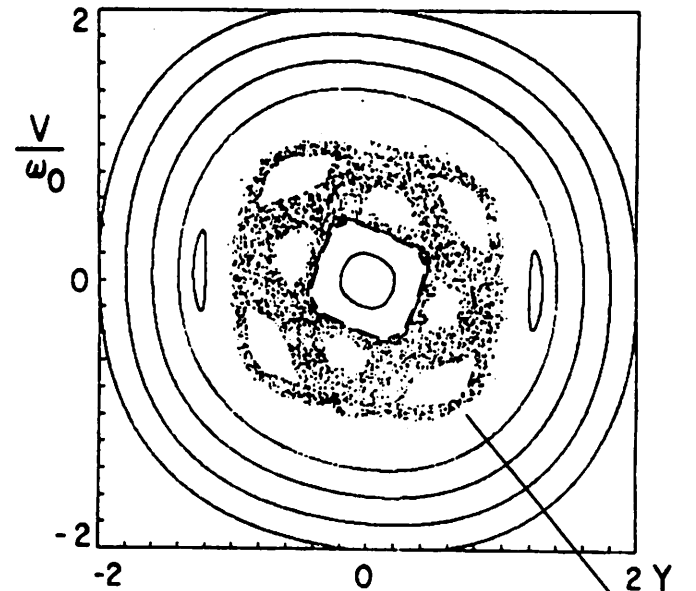


(c) $P_s = 200$

NON-OVERLAPPING

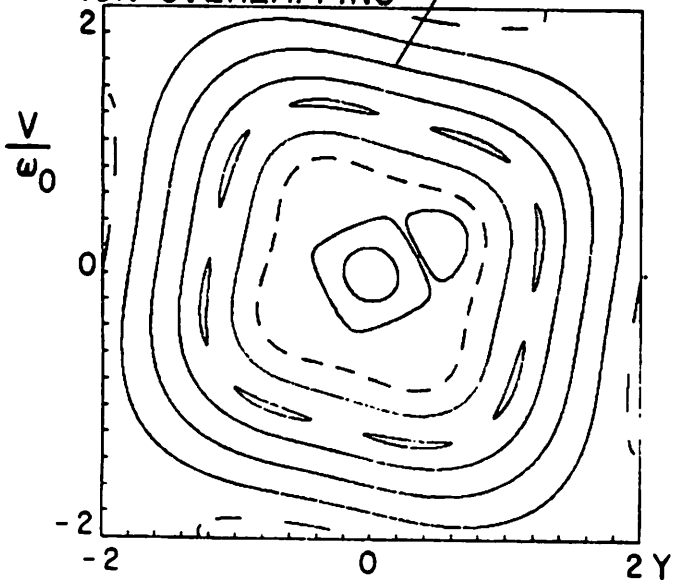


(a) $P_s = 50 = 1/\Omega$

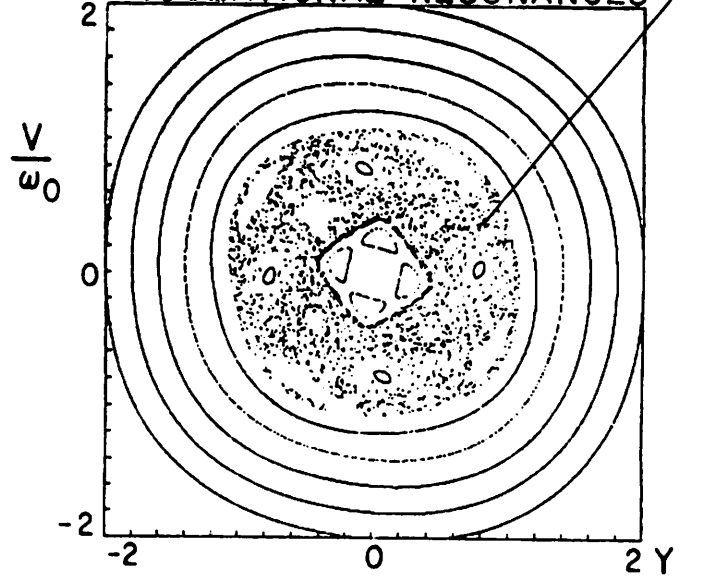


OVERLAPPING OF MODULATIONAL RESONANCES (d) $P_s = 400$

NON-OVERLAPPING



(b) $P_s = 100$



(e) $P_s = 600$

